JURASSIC-RECENT STRUCTURE, STRATIGRAPHY, AND BASIN MODELING OF THE RIFTED-PASSIVE MARGIN OF SOUTHERN MOROCCO

by
Tarek Mohamed Ibrahem Ali Galhom

A thesis submitted to the Department of Earth and Atmospheric Sciences,
College of Natural Sciences and Mathematics
in partial fulfillment of the requirements for the degree of

Master of Science

in Geology

Chair of Committee: Paul Mann

Committee Member: John Suppe

Committee Member: Kurt Rudolph

University of Houston
May 2020

DEDICATION

To my family

ACKNOWLEDGMENTS

I thank Dr. Paul Mann for his guidance and supervision of this master's thesis, for accepting me on as an MS thesis student in my second year, and for suggesting to me this study of the Moroccan rifted-passive margin as a thesis topic. I thank Dr. John Suppe for providing his graduate structure course and for his many insights into the structure of this study area. I also thank Kurt Rudolph for serving on my committee and for his many contributions to this study especially in the areas of seismic interpretation, sequence stratigraphy, and basin modeling.

I thank the Fulbright Scholarship Committee in Egypt for selecting me as a Fulbright fellowship and for providing me two years of full financial and travel support as a master's student at the University of Houston. I thank Robert Sorley and Dr. Jeniffer Masy of Geoex Ltd. and the managers of ONHYM, the National Office of Hydrocarbons and Mines of Morocco, for granting me access to their offshore seismic reflection dataset that formed the basis for this master's thesis and their suggestions for the thesis study.

Special thanks to Alan Nunns, Nathan Eichelberger, and Peter Hargrove of Structure Solver, LLC, for their assistance in applying their software to better understand the structures in this area. I greatly appreciate the friendship, encouragement, and technical support from the post-docs, graduate students, and undergraduate students of the CBTH group that included: Dr. Lei Sun, Nawaz Bugti, Jack Kenning, Sean Romito, Hualing Zhang, Mei Liu, Marcus Zinecker, Bryan Moore, Matthew Storey, Benjamin Miller, and Jacob Miller.

I thank my father, Mohamed Galhom, and brothers in Egypt for their love and encouragement during my last two years in Houston. Most of all I, would like to thank my wife, Salma and our young son Tayim, who have both supported me during these past two years and have patiently put up with my long absences from them in Egypt. Here at UH, I have especially appreciated the support of my friend and fellow graduate student, Aydin Shahtakhtinskiy.

ABSTRACT

The Tarfaya-Dakhla Basin (TDB) is located in the southern part of the Moroccan Atlantic rifted-passive margin. Oblique rifting with its conjugate margin in eastern Canada started at the Late Triassic-Early Jurassic by splitting of the northeast, structural grain inherited from the late Paleozoic, Appalachian-Atlas orogeny. A massive, 14-km-thick, reefal-carbonate platform was formed above the rifted margin during the Early Jurassic and was buried by the 6-km-thick, Early Cretaceous (Berriasian) Boujdour deltaic complex. Continued high rates of clastic sedimentation resulted in margin steepening and gravitational collapse during the Valanginian, to form a 480-km-long and 68-km-wide passive margin fold belt system. This deformed segment of the passive margin includes an up-dip, extensional listric fault zone that passes downslope into a down-dip, folded zone. This study of the Tarfaya-Dakhla basin includes stratigraphic mapping of 4885-line km of depth-converted industry seismic data that are tied to three DSDP wells in the deepwater part of the study area along with published exploratory wells on the slope and shelf.

The results of the study are based on regional isopach and structural maps of Jurassic, Berriasian, Valanginian, Lower, and Upper Cretaceous that range from top oceanic and continental basement to the seafloor. Landward dips in the top basement surface are linked to localized loading by the Jurassic carbonate margin and its overlying Boujdour deltaic complex. Mapping of the passive margin fold belt revealed the updip extension zone to be 480 km long and 30 km wide and the downdip compressional zone to be 117 km long and 15 km wide. The basal detachment beneath the zones of updip extension and downdip compression is estimated from area depth strain analysis to be at a depth of ± 9900 m. Geochemical data from DSDP 397 and 369 wells, and two

pseudo-wells were used to evaluate source rock potential and hydrocarbon prospectivity in the Jurassic to Recent section. Results showed that the Jurassic source rocks are overmature in the study area with hydrocarbon generation beginning in the Upper Jurassic-Lower Cretaceous. The Lower Cretaceous source rocks are immature except for localized areas, and the Upper Cretaceous is immature basin wide.

TABLE OF CONTENTS

DEDICATION ii

ACKNOWLEDGMENTS iii

ABSTRACT v

TABLE OF CONTENTS vii

LIST OF FIGURES ix

1. Introduction and significance of the study 1

2. Tectonic and geologic history of the rifted-passive margin of Morocco 5

2.1 Mesozoic rifting of northwest Africa 5

2.2. Continent-ocean transition in southern Morocco and resulting crustal types beneath the TDB 7

2.3. Moroccan continent-ocean boundary and early magnetic anomalies in transitional or oceanic crust 12

2.4. Stratigraphy of the post-rift passive margin of southern Morocco 13

3. Dataset used and methods for this study 19

3.1 Well data 19

3.2 Seismic reflection data used in the study 21

3.3 Methods used in this study 22

4. Results of this study 23

4.1 Interpreted seismic profiles through the Tarfaya-Dakhla basin 23

4.2 Subsurface mapping of the Moroccan Middle Atlantic passive margin 30

4.2.1 Rifted basement geometry, subsidence, and total sedimentary thickness 30

4.2.2 Jurassic carbonate platform.....32

4.2.3 Mesozoic clastic sediment supply, delta formation, gravitational collapse, and passive margin formation 34

4.2.4 Upper Cretaceous slope front erosion.....38

4.3 Estimation of the detachment depth using the area-depth-strain (ADS) analysis 40

4.3.1 Application of ADS at the down-dip thrusts zone of the PMFB 41

4.3.2 Applying ADS at the regional extension and compression zones of the PMFB ...43

4.4 Basin modeling at the Tarfaya Dakhla basin.....46

4.4.1 Data used for basin modeling 46

4.4.2 Vitrinite reflectance and total organic carbon content of potential source rocks ..48

4.4.3 Basin model boundary conditions.....50

4.4.4 Basin modeling results.....50

5. Discussion 61

6. Conclusions..... 66

BIBLIOGRAPHY 68

LIST OF FIGURES

Figure 1 Regional crustal framework of the Moroccan Atlantic rifted-passive margin showing its three, major rifted-passive margin segments that are conjugate with eastern Canada: 1) **Northern Central Atlantic**; 2) **Georges Bank-Tarfaya Central Atlantic**, and; 3) **Southern Central Atlantic** (three zones modified from Nemcok et al., 2005). The dashed white box shows the study area for this MS thesis located in the Georges Bank-Tarfaya Central Atlantic segment of the Morocco rifted-passive margin. Source of bathymetry is from World Ocean Basemap from Esri et al. (2014), and the topography is from GEBCO (2009) Oceanic crust of the central Atlantic Ocean is shown with early Cretaceous magnetic anomalies from Labails et al. (2009). The zone between the dashed black lines is rifted transitional crust based on the refraction line by Klingelhoefer et al. (2009) that is shown in Figure 3. The blue line represents the seaward edge of the Jurassic carbonate shelf margin extension offshore Morocco from ONHYM (2019). The light red polygon in the north represents the extent of Jurassic salt along the northern Morocco margin from Davison (2005). The black curved line with ages represents the changing positions of the Canary hotspot track (black dots) from 60 Ma to the present from Neumaier et al. (2016)……3

Figure 2 Regional magnetic anomaly map of the Tarfaya Dakhla segment of the Moroccan rifted-passive margin compiled from the EMAG v. 3 magnetic dataset from Meyer et al. (2016). In my study area, I overlay the depth to top continental basement contours in meters based on my mapping. A broad magnetic high parallel to the Morocco shoreline includes the West Atlantic Coast Magnetic Anomaly **(WACMA)**, as compiled from Labails et al. (2009). The African Blake spur Magnetic Anomaly **(ABSMA)** is located 75 km to the west, as mapped by Sahabi et al. (2004). The anomalous magnetic low parallel to the coastline represents deeply subsided, continental basement with up to 19 km of sediment thickness that was called the Cape Boujdour Marginal Rift by Von Rad and Einsele (1980). The anomalous magnetic high at 300 km to the west corresponds to a broad, elongated basement high that extends in a northeast-southwest direction between the Canary Islands in the north and Cape Verde in the south that has been described by Holik et al. (1991). Crustal interpretation from the south to the question marks is from Klingelhoefer et al. (2009), from the question marks to the north is from magnetic data and seismic profile in Figure 6……. 9

Figure 3 Geological-geophysical transect of the Moroccan Atlantic passive margin offshore Dakhla based on refraction and gravity modeling by Klingelhoefer et al. (2009) (location of the cross-section is shown on the map in Figure 1). The section distinguishes five crustal types based on differences in seismic velocity, density, and top basement roughness; **1) Full thickness, continental crust** is 27 km thick and composed of two modeled layers of almost the same thickness (12 and 15 km). **2) Zone of crustal thinning** is underlain by 8-km-thick continental at beneath the continental slope. The velocity values of the upper layer are average for a thinned continental crust, but the lower part shows higher velocities than the full thickness continental crust likely reflecting the presence of magmatic underplating or intrusions in the continental crust formed during the initial breakup (Weigel et al., 1982). **3) Zone of crust of unknown composition** shows velocity values are higher than typical oceanic crust and exhibits a blocky, upper basement surface. Crustal composition was inferred to be either a thin oceanic crust with high serpentinite concentration or an exhumed serpentinized mantle. **4) High-velocity oceanic crust** is an oceanic crust with a smooth basement surface with a slightly higher velocity than the typical oceanic crust that may be related to a lower mantle temperature anomaly during its formation. **5) Normal oceanic crust** is a typical oceanic crust with a rough basement surface and standard velocity. According to Klingelhoefer et al. (2009), the transformation between high-velocity oceanic crust into a typical oceanic crust may reflect different seafloor spreading velocities from Klingelhoefer et al. (2009)..... 10

Figure 4 Summary chart for the Tarfaya Dakhla basin showing geologic time scale, lithostratigraphy, controlling tectonic events and interpreted horizons modified from Nemcok et al. (2005) and Davison (2005). Rifting between the Moroccan Atlantic margin and its conjugate, the Nova Scotia started in the Late Triassic as shown by the development of the onshore half-grabens in Morocco filled by red beds. **Breakup unconformity** and **thermal sag phase** occurred during the Lower Jurassic Hettangian age. **Passive margin phase** began during the Toarcian (191 Ma) or Bajocian (175 Ma) (Klitgord and Schouten, 1986; Srivastava and Tapscott, 1986) and continued through the Cenozoic (Neumaier et al., 2016). **CAMP** (Central Atlantic Magmatic Province) is an extensive, regional magmatic expressed as flows, dikes, and sills during the early Triassic that lasted for only one million years. CAMP occurred approximately 25 Ma following the initiation of central Atlantic rifting (Olsen et al., 2003)..... 16

Figure 5 Stratigraphic correlation of the DSDP and published exploratory wells used in this study modified from Von Rad and Wissman (1982). The yellow line on the inset map shows the location of the A-A' geologic cross-section that passes through **DSDP 139** on the intermediate rise; **DSDP 397** on the uppermost rise**; DSDP 369** on the slope; **Spansah 51 A-1** on the shelf; and **Alisio 15 A-1** on the inner shelf……..... 20

Figure 6 **A.** Uninterpreted, northwest-southeast trending regional seismic profile intersecting Pseudo-1 well (seismic line location is shown in Figure 2). **B.** Interpreted seismic profile at the northern part of the TDB showing the up-dip zone of extension and the down-dip zone of compression that includes the down-dip thrusts zone…….….. 25

Figure 7 **A.** Uninterpreted, northwest-southeast trending seismic profile intersecting DSDP 139 well (location of seismic lines is shown in Figure 2). **B.** Interpreted seismic profile showing the significant change in the basin architecture at the southern part of TDB where the listric normal faults are absent. The upper section of the Lower Cretaceous (probably Albian) shows a basinward thickening and onlapping updip towards the slope forming a basin floor fan. These fans are likely composed of Lower Cretaceous turbidites, which are one of the main reservoirs offshore Dakhla area, according to ONHYM (2019). The thickness of the Upper Cretaceous increases in the southern part of the TDB basin (Figure 12.B). On this profile, the Upper Cretaceous shows a basinward thinning and downlap above the older sediments and likely represents slope fan or distal deltaic deposits.…….…… 29

Figure 8 **A.** Top basement depth structure map showing the subsiding margin in the northeastern part of the basin at the Cape Boujdour marginal rift defined by Von Rad and Einsele (1980). The basement high in the eastern area is close to the WACMA from Klingelhoefer et al. (2009). **B.** Total sediments isopach map showing the thickness variation across the study area with the greatest sediment thickness along the northeastern part at the Cape Boujdour marginal rift and with the thickness decreasing in a southward direction.……...…… 31

Figure 9 **A.** Top Jurassic depth structure map showing the extension of the carbonate platform in the eastern part of the Tarfaya Dakhla basin. The blue line delineates the extension of the Jurassic shelf margin **B.** Jurassic isopach map showing the increase in sediments thickness in the northeastern part of the

study area where the Jurassic sediments filled the area of the proposed Cape Boujdour marginal rift (Von Rad and Einsele, 1980)..... 33

Figure 10 **A.** Top Berriasian depth structure map showing listric normal faults striking northeast-southwest within the updip extension zone of the passive margin fold belt. A roll-over anticline and compressional down-dip thrusts zone define the downdip part of the passive margin fold belt (PMFB)**. B.** Berriasian isopach map showing an increase of sediment thickness within the Berriasian depocenter that is centered in the roll-over anticline..... 35

Figure 11 **A.** Top Lower Cretaceous depth structure map showing the zone of listric normal faults striking northeast-southwest parallel to the slope margin. The density of the listric normal faults is lower at the Lower Cretaceous level as compared to the Berriasian (Figure 10.A). The passive margin fold belt deformation does not extend to the Lower Cretaceous surface. **B.** Lower Cretaceous isopach map showing the maximum sediment thickness within the Lower Cretaceous depocenter in the area of the roll-over anticline. The Berriasian sediment thickness forms a major part of the total Lower Cretaceous thickness..... 37

Figure 12 **A.** Top Upper Cretaceous depth structure map showing a major slope front erosion at the northwestern part of the basin as shown by the grey polygon. This erosion may have been related to a major Oligocene regression that was synchronous with an increase in the Antarctic Bottom Water (AABW). This period of lower sea level would have triggered slumps, submarine canyons, and slope front erosion that eroded as deeply as the Hauterivian as observed in the DSDP 397 well (Arthur et al., 1979; Shipboard Scientific Party, 1979; von Rad and Wissmann, 1982). The black dotted line shows the 60-0 my, margin-parallel track of the Canary Islands hotspot. **B.** Upper Cretaceous isopach map showing the Upper Cretaceous depocenter is centered in the southern part of the basin at Pseudo-2 well. The Upper Cretaceous thickness decreases towards the northwest..... 39

Figure 13 Application of area-depth-strain analysis (ADS) to measure the deeply buried, depth to detachment beneath the down-dip thrusts zone. The solid yellow vertical axis represents the depth, and the colored squares represent the excess area values at each layer. The ADS analysis indicates a general increase in excess area upwards through the pre-growth layers (that include the zone from Layer 1 to the Valanginian). There is no decreasing trend at the upper layers, which indicates the absence of growth strata during this period. Based on ADS, the interpreted depth to detachment is ± 9900 m, while the best-fit detachment depth is ± 10300 m. This predicted zone of

detachment may reflect the loss of area at the shaly, ductile layers due to thickening, which violates the ADS analysis that is based solely on the conservation of area. More detailed interpretation of the best-fit line shows that the possibility of three, smaller, best-fit lines indicative of a zone of three detachments rather than a single detachment: 1) From Jurassic to layer 2, 2) From layer 3 to layer 7, and 3) from Berriasian to Valanginian. Values at each layer include: 1) best-fit displacement, 2) nominal displacement, and 3) layer parallel strain.…… 42

Figure 14 Application of area-depth-strain analysis (ADS) to estimate the detachment depth based on the regional extension and compression of the passive margin fold belt. The colored squares represent the excess area value for each horizon. The shaded area under the regional datum at the Berriasian horizon represents the extension in positive values, while the compression above the datum is shown as negative values. The net displacement from the best-fit is -3869 m, which indicates that the system exhibits more compression than extension that may reflect a deeper folding mechanism. Values at each layer include: 1) best-fit displacement, 2) nominal displacement, and 3) layer parallel strain. The depth of the best-fit detachment is similar to the interpreted detachment at ± 9900 m depth…….…..…. 45

Figure 15 **A.** Modeled versus measured vitrinite reflectance in DSDP 397 well showing the deflection at the top Hauterivian unconformity at 4207 m that is produced by 1400 m of late Cretaceous slope front erosion. **B.** Modeled versus measured temperature values with modeled vitrinite reflectance overlay. (**Blue color** = immature; **green color** = oil window; **red color** = gas window; and **yellow color** = over-mature). Potential Hauterivian source rocks have been documented from core samples to be immature in the DSDP 397 well.……...…….. 52

Figure 16 Burial history versus transformation ratio for the basin modeling sites at DSDP well 397, at DSDP well 369, Pseudo-1, and at Pseudo-2 modeling sites. **A**. The maximum subsidence rate occurred between 150 to 130 Ma at the DSDP 397 well. **B.** The maximum subsidence rate occurred between 150 to 130 Ma at the DSDP 369 well and is similar to the period of maximum subsidence at the DSDP 397 well. **C.** The highest, modeled subsidence rate occurred between 210-135 Ma at the Pseudo-1 modeling site. **D.** The subsidence rate observed at the Pseudo-2 modeling site is lower than the other sites. The modeled transformation ratio indicates that Jurassic source rocks generated hydrocarbons early but are presently overmature in the Tarfaya Dakhla basin. A potential Hauterivian source is currently within its late generative stage at the Pseudo-1 and Pseudo-2 modeling sites. The

Albian source rocks are only within the late generative stage at the Psuedo-2 modeling site. The Campanian source rocks are generally immature..... 55

Figure 17 Vitrinite reflectance and transformation ratio versus time for the middle section of the Middle Jurassic at the Pseudo-1 modeling site and the middle section of the Lower Jurassic at the DSDP 397 well, at the DSDP 369 well, and at the Pseudo-2 modeling sites. **A.** Hydrocarbon generation of the Lower Jurassic occurred between 170-140 Ma at DSDP well 397. **B.** Hydrocarbon generation of the Lower Jurassic at the DSDP 369 well occurred between 170-140 Ma. **C.** Hydrocarbon generation of the middle Jurassic at the Pseudo-1 model occurred between 160-145 Ma. **D.** Hydrocarbon generation of the Lower Jurassic at the Pseudo-2 model occurred between 140-80 Ma. Jurassic source rocks are currently overmature (Ro>2.0) at the four modeling sites: DSDP well 397, DSDP 369, Pseudo-1 well, and Pseudo-2 well modeling site.…….…… 58

Figure 18 Vitrinite reflectance and transformation ratio versus time of the Hauterivian section at the modeling sites of DSDP well 397, DSDP well 369, Pseudo-1 well, and Pseudo-2 well. **A.** Modeling results at the DSDP 397 well show that there is no significant maturation and generation. **B.** Modeling results at the DSDP 369 well show that there is no considerable maturation and generation as was also modeled at the DSDP 397 well. **C.** Modeling results at the Pseudo-1 model show that the potential Hauterivian source is currently generative and within the gas window with generation having begun during the Upper Cretaceous. **D.** Modeling results at the Pseudo-2 model show that the potential Hauterivian source is currently generative and within the gas window. Generation began during the Paleocene……...…… 60

Figure 19 Regional 2D seismic profile across the study area summarizing the extent and depth ranges of the present-day oil, wet gas, and dry gas windows based on estimates using modeled vitrinite reflectance values from DSDP well 397, DSDP 369, Pseudo-1 well and Pseudo-2 well. The **oil window** is interpreted as 0.6-1.1 Ro, the **wet gas window** as 1.1-1.3 Ro, and the **dry gas window** as 1.3-2.0 Ro. These maturity windows are found at greater depths below the seafloor in the deeper water areas of the study area because of crustal heat flow is lower in areas of oceanic crust, and colder bottom waters are present at those greater water depths……. 64

1. Introduction and significance of the study

The Moroccan rifted-passive margin of the Central Atlantic Ocean extends 3500 km from the Straits of Gibraltar to the border of southern Morocco with Mauritania and forms the conjugate rifted margin for much of eastern margin of the USA and Maritime Canada (Figure 1). Rifting between the Moroccan Atlantic margin and its North American conjugate began in the Late Triassic with the development of grabens and half-grabens filled with clastic red beds on both margins (Davison, 2005). The Atlas Mountains in northern Morocco include the same Jurassic rifts that were inverted during Cenozoic convergence between the African and European plates. A major Jurassic salt province occurs as a locally reactivated, post-rift sag sequence along the northern margin of Morocco (Davison, 2005; Lawrence, 2019). Maillard et al. (2006) have proposed that early rifting of the Central Atlantic was asymmetrical in cross-sectional view with the less extended Moroccan margin representing the narrower upper plate and the much more extended North American plate being part of the lower plate.

Hydrocarbon exploration of the offshore Morocco margin over the past few decades has been disappointing with a series of an unsuccessful shelf, slope, and deepwater wells drilled from the late 1960s through the early 2000s into Lower Cretaceous-Cenozoic clastic rocks and Jurassic carbonate rocks (Von Rad and Wissmann, 1982; ONHYM, 2019; Lawrence, 2019). Deepwater stratigraphic wells completed by the Deep Sea Drilling Project (DSDP) during the mid-to-late 1970s encountered numerous gas and oil and shows which supported the presence of underlying,

Figure 1: Regional crustal framework of the Moroccan Atlantic rifted-passive margin showing its three, major rifted-passive margin segments that are conjugate with eastern Canada: 1) **Northern Central Atlantic**; 2) **Georges Bank- Tarfaya Central Atlantic**, and; 3) **Southern Central Atlantic** (three zones modified from Nemcok et al., 2005). The dashed white box shows the study area for this MS thesis located in the Georges Bank-Tarfaya Central Atlantic segment of the Morocco rifted-passive margin. Source of bathymetry is from World Ocean Basemap from Esri et al. (2014), and the topography is from GEBCO (2009) Oceanic crust of the central Atlantic Ocean is shown with early Cretaceous magnetic anomalies from Labails et al. (2009). The zone between the dashed black lines is rifted transitional crust based on the refraction line by Klingelhoefer et al. (2009) that is shown in Figure 3. The blue line represents the seaward edge of the Jurassic carbonate shelf margin extension offshore Morocco from ONHYM (2019). The light red polygon in the north represents the extent of Jurassic salt along the northern Morocco margin from Davison (2005). The black curved line with ages represents the changing positions of the Canary hotspot track (black dots) from 60 Ma to the present from Neumaier et al. (2016).

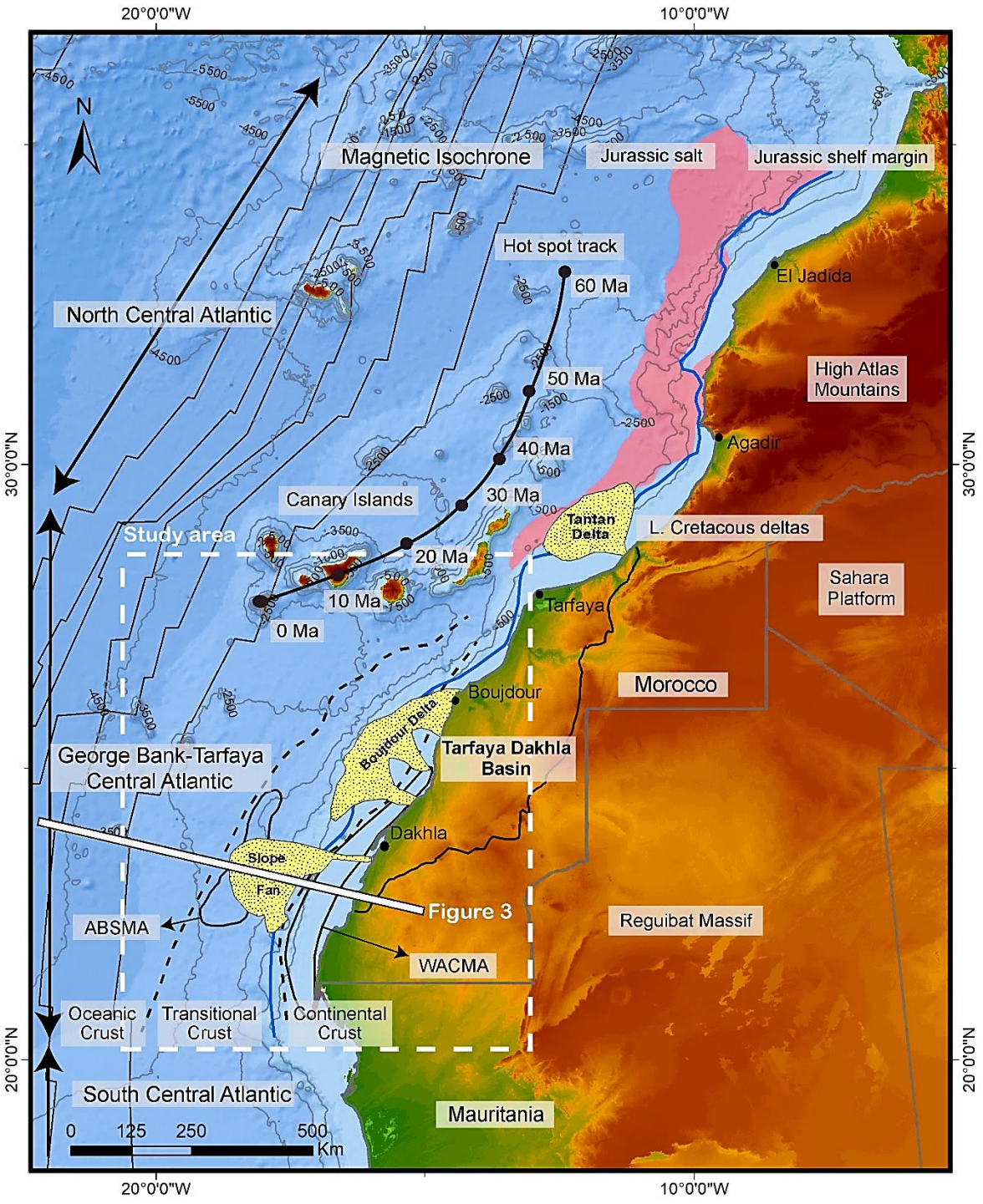
20°0'0"W
10°0'0"W
30°0'0"N
20°0'0"N
N
Magnetic Isochrone
Jurassic salt
Jurassic shelf margin
Hot spot track
60 Ma
50 Ma
40 Ma
30 Ma
20 Ma
10 Ma
0 Ma
North Central Atlantic
Canary Islands
Study area
El Jadida
High Atlas Mountains
Agadir
Tantan Delta
L. Cretacous deltas
Sahara Platform
Tarfaya
Morocco
Boujdour
Boujdour Delta
Tarfaya Dakhla Basin
George Bank-Tarfaya Central Atlantic
Dakhla
Slope Fan
Figure 3
ABSMA
WACMA
Reguibat Massif
Oceanic Crust
Transitional Crust
Continental Crust
South Central Atlantic
Mauritania
0 125 250 500 Km

mature source rocks within the very thick Jurassic-Lower Cretaceous section that has long interested oil explorationists (Hayes et al., 1972; The Shipboard Scientific Party, 1978;Shipboard scientific party, 1979)

Based on the same data sets described in this thesis, Lawrence (2019) revealed the presence of a previously undescribed, 480-km-long passive margin fold belt (Rowan, 2004) within the Tarfaya-Dakhla basin (TDB) of southern Morocco (Figure 1). Passive margin fold belts form as a result of large-scale, thin-skinned, gravity-driven deformations associated with salt or shale detachment surfaces (Rowan, 2004; Krueger and Gilbert, 2009; Morley et al., 2011). Updip deformation is marked by a zone of listric normal faults with associated rollover anticlines that converge onto a single or zone of seaward-dipping detachment faults (Hafid et al., 2008)

On the southern Morocco margin, this localized area of complex deformation within the passive margin fold belt is a likely area of increased structural trapping for the mature, underlying Jurassic-Cretaceous section as seen in other areas like the Gulf of Mexico (Fiduk et al., 1999; Le Roy et al., 2008). Davison (2005) had also recognized this passive margin fold belt and pointed out that rollover anticlines associated with listric, normal faults are important targets for offshore exploration. Davison (2005) noted that the depth to detachment might extend as deeply as the top basement horizon.

Objectives of this study. The main objective of the study is to evaluate the passive margin fold belt in the Tarfaya-Dakhla basin (TDB) in the southernmost part of the Moroccan passive margin and petroleum system modeling of the source rocks. There are few published papers about

the southern margin of Morocco (ONHYM, 2019), especially for this newly recognized passive margin fold belt. In comparison, several passive margin fold belts have been described in detail from the margins of Nigeria, Somalia, and Kenya, where the relation between their formation, timing, and hydrocarbon prospectivity have been studied in detail (Maloney et al., 2012; Cruciani and Barchi, 2016). The grid of depth-converted seismic data provided by Geoex Ltd allows the construction of structural maps and isopach maps that will provide greater precision for structural and stratigraphic interpretation and basin modeling.

2. Tectonic and geologic history of the rifted-passive margin of Morocco

2.1 Mesozoic rifting of northwest Africa

Rifting along the Moroccan Atlantic margin was oriented north-northeast and followed the trend of the late Paleozoic Hercynian orogenic belt. The Moroccan Atlantic margin is divided into three main segments according to the direction of Triassic-Jurassic rifting: the Northern Central Atlantic segment, the Southern Central Atlantic segment, and the Georges Bank-Tarfaya Central Atlantic segment, where my study area is located (Nemcok et al., 2005) (Figure 1).

Early Central Atlantic rift history. According to (Nemcok et al., 2005), the direction of Triassic-Jurassic rifting in the Northern and Southern segments of the Moroccan margin was perpendicular to the margin and formed extensional, margin-parallel, grabens and half-grabens. In contrast, rifting in the Georges-Bank-Tarfaya segment was highly oblique because of the irregular shape of this part of the margin and formed a left-lateral, strike-slip regime that included the Gettysburg-Tarfaya and Georges Bank-Tarfaya strike-slip zones. Triassic, continental rifting and

basin formation in this southern area of the Moroccan margin has been interpreted as occurring within strike-slip-related, pull-apart basins (Nemcok et al., 2005)(Figure 1).

Continental basement and early rifting of the Tarfaya Dakhla basin. Using isostatic, residual gravity anomaly data to map the basement structures, Nemcok et al. (2005) inferred that the continental crust underlying the Tarfaya Dakhla basin is underlain by several continental, fault blocks with complex geometries. These fault blocks have average widths and lengths of 20-30 km and 30-100 km, respectively, and are marked by steep gravity gradients. The interpreted fault blocks have abrupt boundaries and are elongated in a northeast-southwest direction.

Rift-related, Mesozoic sedimentation. During the Triassic and Lower Jurassic rifting event, rift basins were filled with alluvial and lacustrine sediments with minor salt precipitation near the area of the northern TDB (Lawrence, 2019). Although isolated salt diapers have been reported by previous workers above this zone of rifting in southern Morocco (Davison and Dailly, 2010; ONHYM, 2019), the main area of salt deposition is located along the rifted, northern margin of Morocco (Lawrence, 2019) (Figure 1). The Geoex Ltd. seismic data that was made available for this study does not penetrate deeply enough to image these deeply buried continental basement blocks or rift and pull-apart basins, so this phase of the early opening was not a focus of this study.

Triassic CAMP magmatic event. The Central Atlantic Magmatic Province (CAMP) is a widespread Mesozoic igneous event related to a mantle plume that is well-dated as early Triassic (201 Ma). It lasted only about 1 million years, and post-dated the initial rifting along the two, conjugate margins by 25 million years (Davison and Dailly, 2010). The CAMP event is marked

by an area of basaltic and radial dikes, sills, and thick sequences of layered flows "seaward-dipping reflectors" along the rifted margins of Central Atlantic in northwestern Africa, the eastern USA, and northeastern South America. In northwestern Africa, evaporites were formed above and within the CAMP magmatic units, which suggests the existence of a large, salt-filled sag basin with the absence of significant uplift before or during the CAMP event at 201 Ma (Davison, 2005). My seismic data does not penetrate deeply enough to establish whether CAMP magmatism affected this segment of the Moroccan margin; therefore, this topic does not form a focus of this study.

2.2. Continent-ocean transition in southern Morocco and resulting crustal types beneath the TDB

Klingelhoefer et al. (2009) used refraction, gravity, and velocity data to distinguish five major, crustal types underlying the TDB based on their observations of seismic velocity, crustal densities, and the roughness of the top basement surface. The five underlying crustal zones of the TDB are summarized on the cross-section in Figure 3 that was modified from Klingelhoefer et al. (2009). The limits of the zone of thinned continental crust and the zone of crust of unknown composition are shown on the map in Figure 2. These five zones are:

1) Zone of full-thickness continental crust. The thickness of this easternmost crustal zone of the northwestern Africa craton is ~27 km and includes two modeled layers of almost the same thickness (12 and 15 km**).**

Figure 2: Regional magnetic anomaly map of the Tarfaya Dakhla segment of the Moroccan rifted-passive margin compiled from the EMAG v. 3 magnetic dataset from Meyer et al. (2016). In my study area, I overlay the depth to top continental basement contours in meters based on my mapping. A broad magnetic high parallel to the Morocco shoreline includes the West Atlantic Coast Magnetic Anomaly **(WACMA)**, as compiled from Labails et al. (2009). The African Blake spur Magnetic Anomaly **(ABSMA)** is located 75 km to the west, as mapped by Sahabi et al. (2004). The anomalous magnetic low parallel to the coastline represents deeply subsided, continental basement with up to 19 km of sediment thickness that was called the Cape Boujdour Marginal Rift by Von Rad and Einsele (1980). The anomalous magnetic high at 300 km to the west corresponds to a broad, elongated basement high that extends in a northeast-southwest direction between the Canary Islands in the north and Cape Verde in the south that has been described by Holik et al. (1991). Crustal interpretation from the south to the question marks is from Klingelhoefer et al. (2009), from the question marks to the north is from magnetic data and seismic profile in Figure 6.

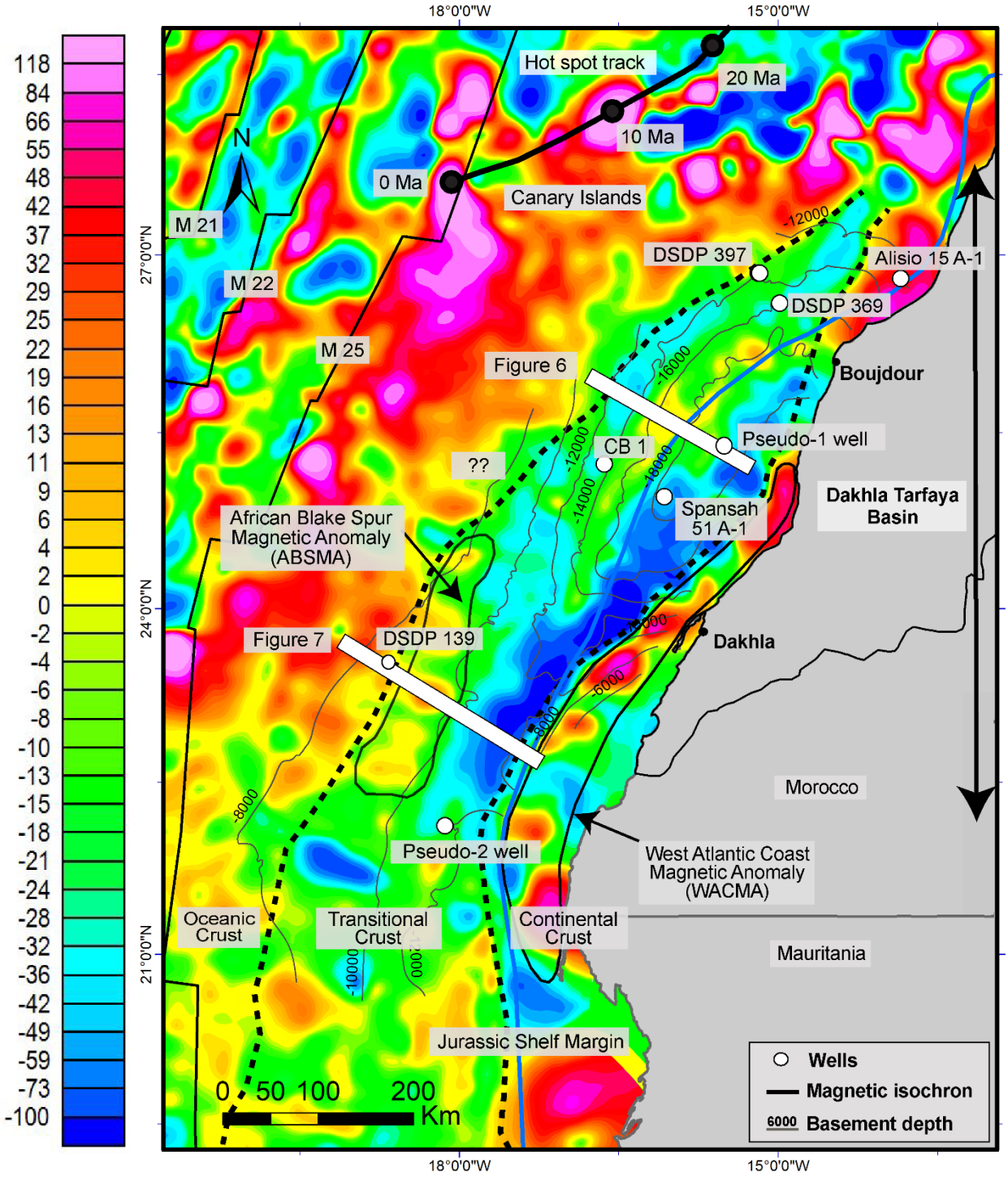
118
84
66
55
48
42
37
32
29
25
22
19
16
13
11
9
6
4
2
0
-2
-4
-6
-8
-10
-13
-15
-18
-21
-24
-28
-32
-36
-42
-49
-59
-73
-100
18°0'0"W
15°0'0"W
27°0'0"N
24°0'0"N
21°0'0"N
N
Hot spot track
20 Ma
10 Ma
0 Ma
Canary Islands
M 21
M 22
M 25
DSDP 397
Alisio 15 A-1
DSDP 369
Figure 6
Boujdour
Pseudo-1 well
CB 1
??
Spansah
51 A-1
Dakhla Tarfaya
Basin
African Blake Spur
Magnetic Anomaly
(ABSMA)
Figure 7
DSDP 139
Dakhla
Morocco
Pseudo-2 well
West Atlantic Coast
Magnetic Anomaly
(WACMA)
Oceanic
Crust
Transitional
Crust
Continental
Crust
Mauritania
Jurassic Shelf Margin
0 50 100 200
Km
Wells
Magnetic isochron
6000 Basement depth

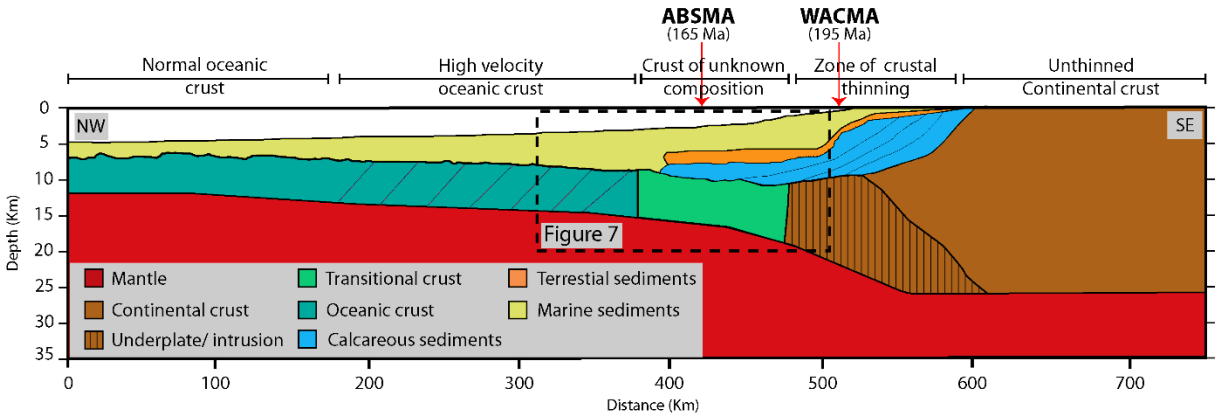

Figure 3: Geological-geophysical transect of the Moroccan Atlantic passive margin offshore Dakhla based on refraction and gravity modeling by Klingelhoefer et al. (2009) (location of cross-section is shown on the map in Figure 1). The section distinguishes five crustal types based on differences in seismic velocity, density, and top basement roughness; **1) Full-thickness continental crust** is 27 km thick and composed of two modeled layers of almost the same thickness (12 and 15 km). **2) Zone of crustal thinning** is underlain by 8-km-thick continental at beneath the continental slope. The velocity values of the upper layer are average for a thinned continental crust, but the lower part shows higher velocities than the full thickness continental crust likely reflecting the presence of magmatic underplating or intrusions in the continental crust formed during the initial breakup (Weigel et al., 1982). **3) Zone of crust of unknown composition** shows velocity values are higher than typical oceanic crust and exhibits a blocky, upper basement surface. Crustal composition was inferred to be either a thin oceanic crust with high serpentinite concentration or an exhumed serpentinized mantle. **4) High-velocity oceanic crust** is an oceanic crust with a smooth basement surface with a slightly higher velocity than the typical oceanic crust that may be related to a lower mantle temperature anomaly during its formation. **5) Normal oceanic crust** is a typical oceanic crust with a rough basement surface and standard velocity. According to Klingelhoefer et al. (2009), the transformation between high-velocity oceanic crust into a typical oceanic crust may reflect different seafloor spreading velocities from Klingelhoefer et al. (2009).

2) Zone of crustal thinning and underplating. In this wedge-shaped zone of continental crustal thinning, there is a progressive decrease from the full-thickness, 27-km-thick crust to a reduced thickness continental crust of 8 km beneath the continental slope (Figure 3). The velocity values of the upper layer are typical for a thinned continental crust, but the lower shows higher velocities than the adjacent, 27-km-thick, full-thickness crust. The high velocity of the thinned lower crust indicates the presence of magmatic underplating or high-density intrusions into the lower, continental crust that occurred during initial rifting (Weigel et al., 1982; Klingelhoefer et al., 2009).

3) Zone of a crust of unknown composition. In this zone underlying the deep basin, the velocity values are higher than the typical oceanic crust and exhibit a blocky basement surface (Figure 3). Klingelhoefer et al. (2009) propose that this zone is either composed of thin oceanic crust with high serpentinite concentration or consists of exhumed serpentinized mantle.

4) Zone of high-velocity oceanic crust. This zone consists of 6-8 km thick oceanic crust with a smooth top basement surface. Klingelhoefer et al. (2009) propose that it has a slightly higher velocity than typical oceanic crust as a result of a higher temperature of the lower mantle during its formation along a spreading ridge.

5) Zone of normal oceanic crust: This zone is a typical 6-8-km thick oceanic crust with a rough top basement surface and a standard velocity characteristic of oceanic crust. The transition between the adjacent zone of high-velocity oceanic crust into this zone of the typical oceanic crust may have resulted from an increase in seafloor spreading velocities (Klingelhoefer et al., 2009).

2.3. Moroccan continent-ocean boundary and early magnetic anomalies in transitional or oceanic crust

In order to provide a more regional view of the continent-ocean transition beneath the TDB, maps of bathymetry and magnetic anomalies in the zone of normal oceanic crust of northwest Africa and the adjacent zones of thinned continental crust and full-thickness continental crust are shown on Figures 1 and 2.

East Coast magnetic anomaly vs. West African Coast magnetic anomaly. The most continuous and robust anomaly on the eastern North American conjugate margin of Morocco is the East Coast Magnetic Anomaly (ECMA) that was first described by Keller et al. (1954) in the offshore area of Nova Scotia. Later studies have confirmed that the edge of the ECMA delineates the continental oceanic boundary along the coasts of both Canada and the eastern USA (Labails et al., 2010). Refraction and reflection imaging has shown that the ECMA is underlain by thick belts of magnetically-prominent, subaerial lava flows that formed a province of seaward-dipping reflectors (SDRs) along the margin of eastern North America (Austin et al., 1990; Talwani et al., 1995).

In northwest Africa, Sahabi et al. (2004) proposed that West African Coast Magnetic Anomaly (WACMA) is the equivalent anomaly of the ECMA on the North American conjugate margin. However, the WACMA shows some significant differences with the ECMA: 1) WACMA is largely confined to the coastal, full-thickness or slightly seaward area of thinned, continental crust (Figures 1, 2), so the WACMA is located in a more continent ward and less seaward position

than the ECMA on the North American margin; because WACMA extends further north on the African margin than the ECMA extends on the North American margin, so the two do not restore to a single location (Figure 3); 2) WACMA exhibits a weaker, magnetic amplitude than ECMA; 3) existing refraction data for WACMA show no clear association with a thick belt of subaerial, lava flows; instead the magnetic high of WACMA may emanate from a zone of sub-crustal underplating that includes a zone of dikes and sills as shown in the crustal cross-section modified from Klingelhoefer et al. (2009) or, alternatively is related to an elongate, shallow intrusions into the shallow continental crust (Roeser, 1982) (Figure 3).

Blake Spur Magnetic Anomaly. The Blake Spur Magnetic Anomaly (BSMA) is found more distal from the continent edge and around 150-250 km seaward of the ECMA. The age of the oceanic crust east of the BSMA is 165 Ma (Callovian age) (Gradstein et al., 2004). The BSMA is considered to be the product of an eastward ridge jump at 170 Ma. (Labails et al., 2010). The ABSMA correlates with a zone of tilted half grabens filled by volcanic flows (Figure 2).

2.4. Stratigraphy of the post-rift passive margin of southern Morocco

Post-rifting breakup unconformity and sag basin. The breakup unconformity and thermal sagging phase occurred along the margin of southern Morocco during the Lower Jurassic (Hettangian) (Nemcok et al., 2005) (Figure 4). This sag phase terminated the rift phase and heralded the beginning of the Jurassic passive margin phase between North America and Africa that began between the Toarcian (191 Ma) and Bajocian (175 Ma) (Klitgord and Schouten, 1986;

Srivastava and Tapscott, 1986). The Moroccan passive margin phase was long-lived and extended through the Cretaceous and Cenozoic to the present-day (Neumaier et al., 2016) (Figure 4).

Thickness of the passive margin. The average sediment thickness at the passive margin of Morocco is around 9 km in the northern basins and increases to 12-19 in the TDB (ONHYM, 2019) (Figure 1). The thickest area of the passive margin is 19 km thick in the TDB of southern Morocco passive margin that Van Rad and Einsele (1980) called the "Cape Boujdour marginal basin" that they inferred overlay a Triassic-Jurassic rift. Outside of this anomalously thick area, Von Rad and Einsele (1980) estimated a passive margin sediment thickness of 12-14 km.

Lithologies of the underlying African continental basement. The Precambrian, continental basement at the TDB is mainly metamorphic rocks that forms the seaward extension of the Requibat Massif mountains (Figures 1,2). This basement includes metamorphic rocks overlain by a rift-related sequence of terrestrial sandstone, red beds, and conglomerate with minor evaporite deposits (Von Rad and Einsele, 1980) (Figure 4).

Figure 4: Summary chart for the Tarfaya Dakhla basin showing geologic time scale, lithostratigraphy, controlling tectonic events and interpreted horizons modified from Nemcok et al. (2005) and Davison (2005). **Rifting** between the Moroccan Atlantic margin and its conjugate, the Nova Scotia started in the Late Triassic as shown by the development of the onshore half-grabens in Morocco filled by red beds. **Breakup unconformity** and **thermal sag** phase occurred during the Lower Jurassic Hettangian age. **Passive margin** phase began during the Toarcian (191 Ma) or Bajocian (175 Ma) (Klitgord and Schouten, 1986; Srivastava and Tapscott, 1986) and continued through the Cenozoic (Neumaier et al., 2016). **CAMP** (Central Atlantic Magmatic Province) is an extensive, regional magmatic expressed as flows, dikes, and sills during the early Triassic that lasted for only one million years. CAMP occurred approximately 25 Ma following the initiation of central Atlantic rifting (Olsen et al., 2003).

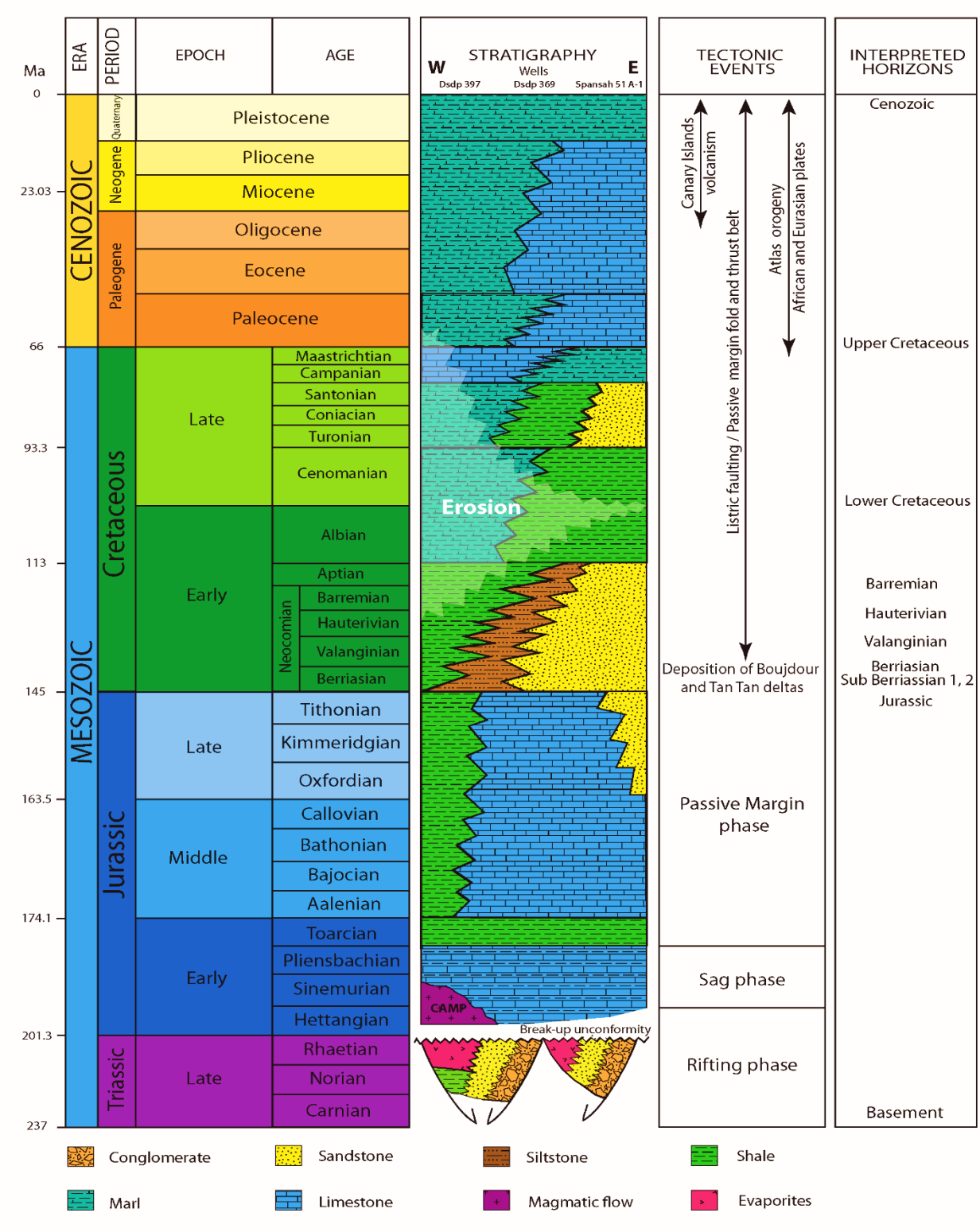
Ma
ERA
PERIOD
EPOCH
AGE
0
23.03
66
93.3
113
145
163.5
174.1
201.3
237
CENOZOIC
MESOZOIC
Quaternary
Neogene
Paleogene
Cretaceous
Jurassic
Triassic
Pleistocene
Pliocene
Miocene
Oligocene
Eocene
Paleocene
Late
Early
Middle
Late
Early
Late
Maastrichtian
Campanian
Santonian
Coniacian
Turonian
Cenomanian
Albian
Aptian
Neocomian
Barremian
Hauterivian
Valanginian
Berriasian
Tithonian
Kimmeridgian
Oxfordian
Callovian
Bathonian
Bajocian
Aalenian
Toarcian
Pliensbachian
Sinemurian
Hettangian
Rhaetian
Norian
Carnian
STRATIGRAPHY
W
Wells
E
Dsdp 397
Dsdp 369
Spansah 51 A-1
Erosion
CAMP
Break-up unconformity
TECTONIC EVENTS
Canary Islands volcanism
Atlas orogeny
African and Eurasian plates
Listric faulting / Passive margin fold and thrust belt
Deposition of Boujdour and Tan Tan deltas
Passive Margin phase
Sag phase
Rifting phase
INTERPRETED HORIZONS
Cenozoic
Upper Cretaceous
Lower Cretaceous
Barremian
Hauterivian
Valanginian
Berriasian
Sub Berriassian 1, 2
Jurassic
Basement
Conglomerate
Sandstone
Siltstone
Shale
Marl
Limestone
Magmatic flow
Evaporites

Triassic-Jurassic evaporite deposits and variable clastic input. The amount of syn-rift clastic sediment input along the Moroccan Atlantic margin likely controlled the presence of evaporite deposits along the margin (Van Rad and Einsele, 1980). The thickness of syn-rift, terrigenous, clastic sediments along the northern Moroccan margin is around 900 m. In contrast, the southern Moroccan margin shows thicknesses of more than 3000 m that fill and extends beyond the zone of continental rifts inferred in that area (Heyman, 1989). Syn-rift, sediment starvation, and slow subsidence rates in the northern basins facilitated the deposition of thick evaporites that contrast to the southern basins where the extreme subsidence rate and sediment supply precluded the evaporites deposition (Heyman, 1989) (Figures 1, 2).

Jurassic carbonate shelf and reef deposits. The post-rift, passive margin sequence initiated with the formation of Middle to Upper Jurassic carbonate reef and shelf facies. The maximum width of the carbonate shelf is 150 km and grades basinward into more clastic, shaly facies (Davison, 2005; Nemcok et al., 2005) (Figure 4).

Lower Cretaceous sedimentation and margin collapse. As a result of major sea-level regression and massive continental sediments supply from the African continent during the Lower Cretaceous, a 1-4 km thick section of continental to marine deltaic sediments was deposited across the Moroccan shelf (Shipboard Scientific Party, 1979; Von Rad and Einsele, 1980; ONHYM, 2019) (Figure 4). This massive sediment supply is formed as a result of the uplift and erosion of the Requibat Shield and Anti-Atlas mountains to the east of the TDB (Davison, 2005) (Figures 1, 2). Lower Cretaceous delta fans known as the Boujdour and Tantan deltas (ONHYM, 2019) formed offshore the TDB and drowned the Jurassic carbonate platform (Von Rad and Sarti, 1986)

(Figure 1). High rates of clastic sedimentation in the Cretaceous and Cenozoic led to over-steepening and gravitational collapse of the TDB (Heyman, 1989; Nemcok et al., 2005; ONHYM, 2019)

Upper Cretaceous sedimentation. During the Upper Cretaceous, a Cenomanian transgression deposited pelagic marl, limestone, chalk, and organic-rich shale across the deepwater part of the TDB (Figure 4). The Upper Cretaceous shows a seaward thickness decrease due to limited terrigenous sediment supply during this period. This slowing period of sedimentation formed the prominent reflector at the Cretaceous-Cenozoic boundary where subsidence was discontinuous, and sedimentation either alternated with erosion or stopped completely (Heyman, 1989).

Paleogene sedimentation. Paleogene sedimentary rocks are generally thin, marine chalk in the study area due to the low influx of clastic sediments during this period (Figure 4). The Eocene section of the coastal area consists of mainly clastic sedimentary rocks that grade upward into sandy, shallow-water Neogene limestone with oyster beds (Davison, 2005) (Figure 4).

By the early Neogene time, the uplift and erosion of the area of the Canary Islands was a response to the passage of the Canary Islands hotspot (Figures 1, 2). This event influenced the sedimentary succession and deposition in the deepwater basin between the Canary Islands and Cape Boujdour (Von Rad and Einsele, 1980).

A significant slope front erosion event documented in DSDP 397 well eroded 1400 m of the section between Hauterivian and Paleocene and was probably related to geostrophic, cold, and

deepwater currents composed of Antarctic Bottom Water (AABW) that began eroding the northern African margin during the Oligocene (22-25 Ma) (Figure 4). A 100 Ma hiatus related to this erosion is well documented in the DSDP 397 well (Shipboard Scientific Party, 1979; Von Rad and Einsele, 1980; von Rad and Wissmann, 1982).

3. Dataset used and methods for this study

3.1 Well data

Five wells that are located on the map in Figure 5 were used to calibrate the seismic profiles and estimate the surface ties: three wells are from publications of the DSDP project and are summarized below and two oil exploration wells by a published report by ONHYM (2019):

1) **DSDP site 139** was drilled in 1971 at a water depth of 3047 m in the middle continental rise; site 139 is 250 km far from the southern Moroccan coast. The well was drilled to a depth of 3712 m that reached the early Miocene age (Hayes et al., 1972).
2) **DSDP site 397** was drilled in 1976; the well lies about 150 km from the coast at 2910 m water depth in the uppermost part of the continental rise. The well was drilled to a total depth 4363 m to the Lower Cretaceous (Hauterivian). The well contains a significant 100 My hiatus along a major, slope front erosion that was eroded deeply (1400 m) into the underlying Mesozoic section (Shipboard Scientific Party, 1979)

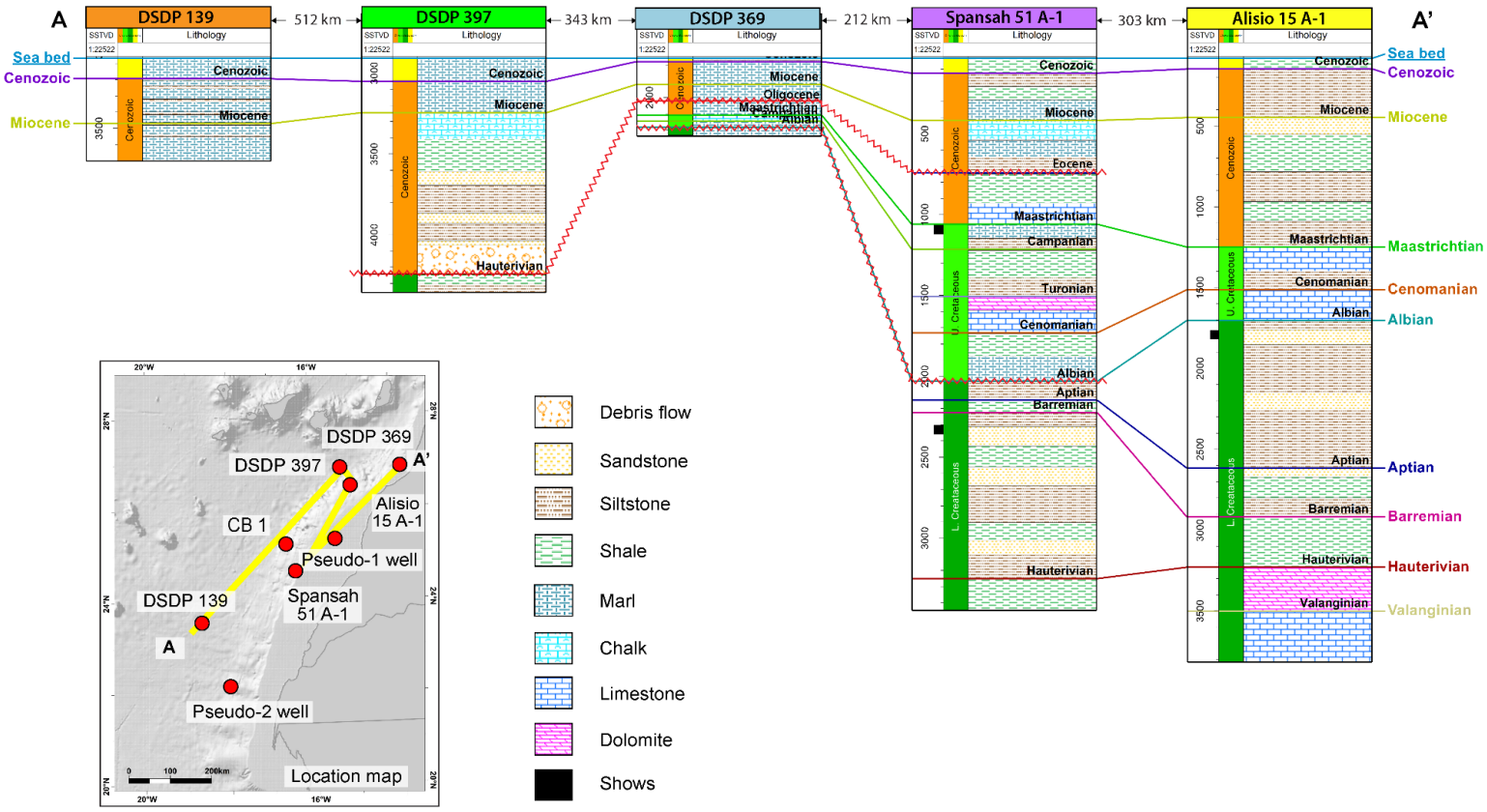

Figure 5: Stratigraphic correlation of the DSDP and published exploratory wells used in this study modified from Von Rad and Wissman (1982). The yellow line on the inset map shows the location of the A-A' geologic cross-section that passes through **DSDP 139** on the intermediate rise; **DSDP 397** on the uppermost rise**; DSDP 369** on the slope; **Spansah 51 A-1** on the shelf; and **Alisio 15 A-1** on the inner shelf.

3) **DSDP site 369** was drilled in 1975; the well lies about 70 km far from the coast at 1752 m water depth on the continental slope. The well total depth is 2240 m at the Aptian and has multiple depositional hiatuses. The most prominent hiatus is the Turonian-Late Albian unconformity (around 16 m. y.) (The Shipboard Scientific Party, 1978) (Figure 5).

Conoco drilled the exploratory well Spansah 51 A-1 in 1969 on the central Moroccan shelf, 120 km from the coast, and in 50 m of water depth (ONHYM, 2019) (Figures 1, 2). The well penetrated the Hauterivian at 3340 m total depth. During the Albian, part of the upper continental slope was eroded (von Rad and Wissmann, 1982). This well encountered oil shows generated in situ from Maastrichtian shaly limestones and gas shows from the Barremian (ONHYM, 2019).

ENPASA drilled the exploratory well Alisio 15 A-1 in 1970 on the shelf, 27 km from the coast, and in 37 m of water depth (Figures 1, 2). The well total depth is 3823 m at the Valanginian (Gesamtfakult et al., 2014), and the well encountered minor gas shows within the Lower Cretaceous section (ONHYM, 2019).

3.2 Seismic reflection data used in the study

The seismic data set used in the study to map the TDB includes 4885 km of depth-converted, and high-resolution, 2D seismic lines that were acquired by Geoex Ltd Company in 2018. The dataset also contains reprocessed legacy seismic lines. Seismic well ties were made

from published reports of the DSDP wells and a public access ONHYM (2019) summary of information on the industry exploratory wells.

3.3 Methods used in this study

Stratigraphy. I used the Geoex Ltd seismic grid from the TDB that totals 4885 km line length to generate structure and isopach maps of the main stratigraphic units in the study area (Figures 1, 2). These maps and surfaces were then used to evaluate the passive margin architecture, its stratigraphic evolution, and its petroleum potential from basin modeling.

Structure. The TDB passive margin fold belt is divided into two structural zones; an up-dip extensional zone with listric faults and a large, roll-over anticline, and a downdip compressional zone with folds and thrusts. Both the updip and downdip zones overlie a single regional detachment surface or, alternatively, a wider zone of multiple detachment surfaces. I applied the method of area-depth-strain analysis to predict the depth of the regional detachment beneath both the extensional and compressional zones.

Basin modeling and hydrocarbon prospectivity. I used the geochemical data of the Jurassic, Lower Cretaceous, Upper Cretaceous sections from the DSDP wells and published literature to evaluate their petroleum prospectivity and maturity in the deepwater part of the study area (Figures 1, 2). Modeling and the creation of two pseudo-wells in areas where wells are not present provided a general overview of the hydrocarbon generation potentiality of the TDB source rocks.

4. Results of this study

4.1 Interpreted seismic profiles through the Tarfaya-Dakhla basin

The Geoex Ltd seismic grid used in this study contains eighteen, widely spaced, depth-converted seismic profiles. Thirteen seismic profiles of 2578 km total line length are oriented northwest-southeast and nearly perpendicular to the structural grain of the rifted margin (Figures 1, 2). Five seismic profiles of 2307 total line length are oriented northeast-southwest and parallel to the modern coastline. Location of the Geoex Ltd seismic grid is not shown in this thesis for confidentiality reasons.

Key horizons of the TDB. Stratigraphic interpretation of the seismic grid from the TDB basin is based on three sources of data: 1) well ties with published DSDP wells (Hayes et al., 1972; The Shipboard Scientific Party, 1978; Shipboard Scientific Party, 1979), 2) published exploratory well reports (ONHYM, 2019), and 3) a comprehensive, public-access, report published by the (Office National Des Hydrocarbures et des Mines) (ONHYM, 2019). Using these ties, I generated depth and isochore maps for nine surfaces in the study area: 1) Top basement; 2) Berriasian; 3) Valanginian; 4) Hauterivian; 5) Barremian; 6) Top Lower Cretaceous; 7) Upper Cretaceous; 8) Base Cenozoic Unconformity, and 9) seafloor (Figure 4).

Structure of the TDB rifted-passive margin. Interpretation of the seismic profile shown in Figure 6 across the northern part of the TDB reflects the complex deformation of the passive margin fold belt system. The top basement horizon in this area is characterized by high-amplitude

seismic reflections produced by the strong impedance contrast between Precambrian crystalline basement rocks and overlying Triassic, clastic sedimentary rocks (Figure 4). The top basement shallows northeastward and is dissected by series of Triassic-Lower Jurassic half-grabens formed by the transtensional rifting of the Precambrian basement (Nemcok et al., 2005).

Jurassic carbonate margin. A major Jurassic carbonate platform was deposited on the top of the rifted basement during a transgressional period (Figures 4, 6). The platform formed a thick package of high-amplitude reflectors at the southeast, that graded to more shaly carbonate rocks in the basinward direction (Sachse et al., 2016) (Figure 6).

Deformed, Cretaceous section. The thick, Lower Cretaceous clastic section is deformed by a group of closely spaced, seaward dipping; listric normal faults formed within a broad, extension zone that soles out into a regional detachment surface along the top Jurassic horizon (Figure 6). These normal faults were active during the Lower Cretaceous and formed, wedge-shaped, rotated fault blocks with their syn-rift, sedimentary thicknesses increasing towards the normal fault surfaces.

The extensional zone is about 50 km wide while the compression zone is about 40 km wide. The transition or "neutral" zone between the extensional and compressional zones is difficult to determine precisely but is centered on the large rollover anticline. Lateral sliding of the listric faults on the detachment surface formed a roll-over anticline, followed by down-dip thrusts at the compression zone. The history of the passive margin fold belt initiated with the regional detachment fault that was later deformed by the younger listric, normal fault.

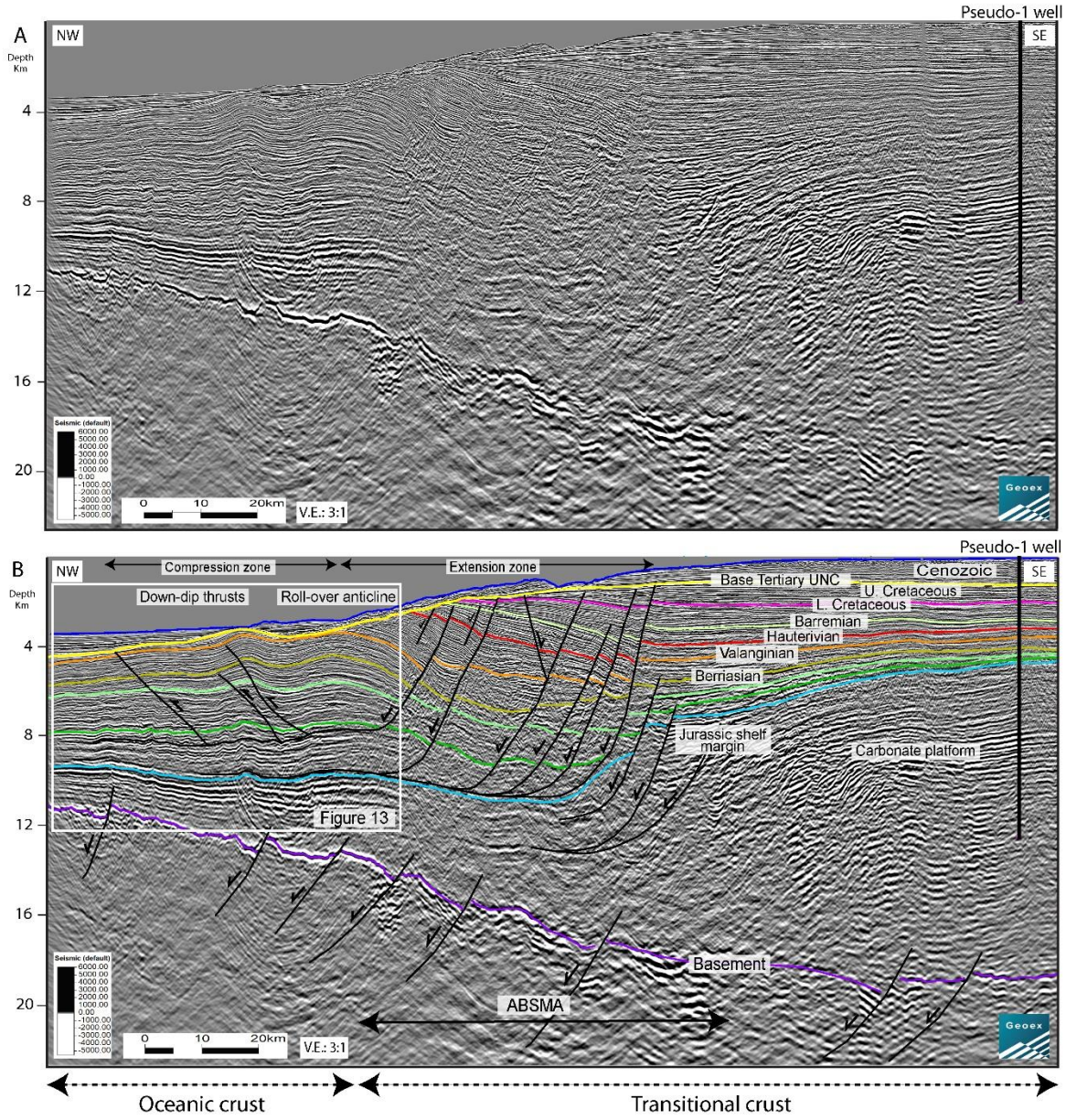

Figure 6: A. Uninterpreted, northwest-southeast trending regional seismic profile intersecting Pseudo-1 well (seismic line location is shown in Figure 2). **B.** Interpreted seismic profile at the northern part of the TDB showing the up-dip zone of extension and the down-dip zone of compression that includes the down-dip thrusts zone.

Upper Cretaceous sedimentation and erosional event. The thickness of the Upper Cretaceous section decreases in the seaward direction due to limited terrigenous sediment supply and erosion that formed the Base Tertiary Unconformity that extends to the shelf (Heyman, 1989) (Figure 4). A significant regression during the Oligocene time was associated with an increase in Antarctic Bottom Water (AABW) flow that produced a series of slumps, submarine canyons, and slope front erosion that eroded 1400 m of the stratigraphic section; this erosion extends to the Hauterivian in the DSDP 397 well (Arthur et al., 1979; Shipboard Scientific Party, 1979; von Rad and Wissmann, 1982) (Fig. 3). Eroded sediments bypassed the slope and re-deposited at the deeper basin floor (Figure 6). According to (Pyles et al., 2011), the slope-basin erosion and re-deposition at the TDB is considered an "out-of-grade type" that is formed during a rapid fall in eustatic sea level.

Relation of underlying crustal types to overlying sedimentation. Crustal interpretation shown on the seismic line in Figure 6 is from my interpretation of magnetic data and seismic features in Figures 2 and 6, respectively, and is similar to the Klingelhoefer et al. (2009) interpretation across the southern part of the TDB near the coastal city of Dakhla (Figure 3). The continental crust lies beneath the WACMA and is 40 km wide (Figure 2). The transitional crust exhibits a blocky basement surface that extends over 120 km; this area of transitional crust includes the ABSMA as shown on the map in Figure 2. The ABSMA is expressed on the seismic line as a group of tilted half-grabens filled with post-rift volcanic flows. The oceanic crust at the northwestern part has a smooth surface and extends over 50 km (Figure 6).

Interpretation of the seismic profile in Figure 7 across the southern part of the TDB shows a significant change in passive margin structure from north to south in a zone where the post-rift, listric normal faults are absent. This change in margin structure likely results from the lower sediment thickness and increased margin stability along the southern margin (9 km) compared to thicker (19 km) along the northern margin where the passive margin is found.

The continental crust offshore the coastal city of Dakhla shows a crustal thickness of 15-20 km with no evidence for subsidence associated with the continental break-up (Figure 3). This lack of subsidence may reflect a thermal uplift process that maintained the thinner crust at a shallow elevation (Labails et al., 2009).

The Jurassic carbonate platform underlies the continental slope offshore of Dakhla (Labails et al., 2009). The profile in Figure 7 includes only the outer edge of the platform. The Lower Cretaceous is thin along the southern part of the basin due to lower sediment supply during this period. The upper part of the Lower Cretaceous (probably Albian) shows a basinward thickening, and onlaps up-dip onto the slope. Cretaceous turbidites forming the basin floor fan are one of the main reservoirs in this area offshore Dakhla (ONHYM, 2019). Where the thickness of the Upper Cretaceous increases in the southern part of the basin, there is a basinward thinning and downlap on older sediments, which may represent a slope fan or distal deltaic deposits (Figure 7).

Figure 7: A. Uninterpreted, northwest-southeast trending seismic profile intersecting DSDP 139 well (location of seismic lines is shown in Figure 2). **B.** Interpreted seismic profile showing the significant change in the basin architecture at the southern part of TDB where the listric normal faults are absent. The upper section of the Lower Cretaceous (probably Albian) shows a basinward thickening and onlapping updip towards the slope forming a basin floor fan. These fans are likely composed of Lower Cretaceous turbidites, which are one of the main reservoirs offshore Dakhla area, according to ONHYM (2019). The thickness of the Upper Cretaceous increases in the southern part of the TDB basin (Figure 12.B). On this profile, the Upper Cretaceous shows a basinward thinning and downlap above the older sediments and likely represents slope fan or distal deltaic deposits.

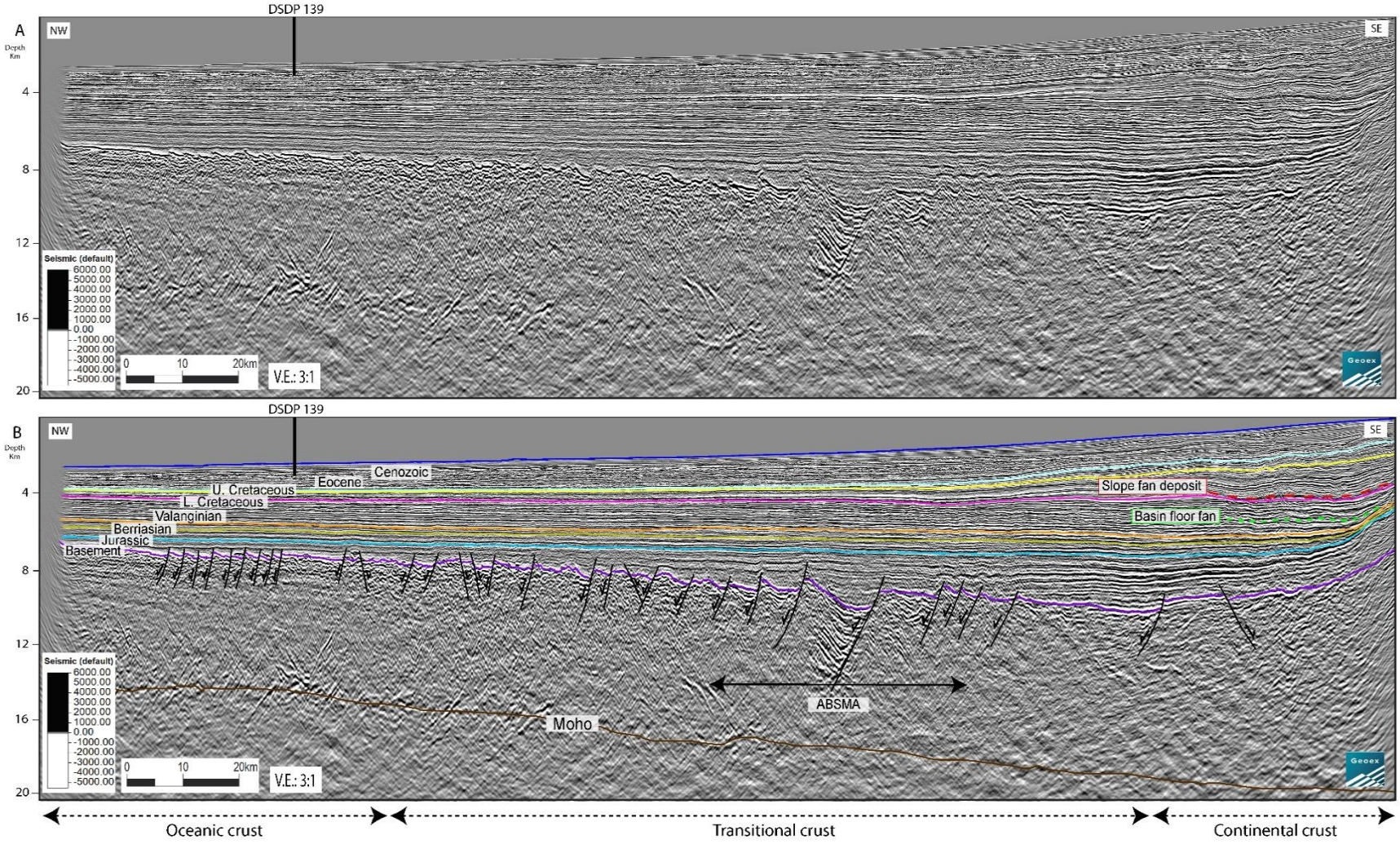
A
Depth Km
NW
SE
DSDP 139
4
8
12
16
20
Seismic (default)
6000.00
5000.00
4000.00
3000.00
2000.00
1000.00
0.00
-1000.00
-2000.00
-3000.00
-4000.00
-5000.00
0
10
20km
V.E.: 3:1
Geoex
B
Depth Km
NW
SE
DSDP 139
Cenozoic
Eocene
U. Cretaceous
L. Cretaceous
Valanginian
Berriasian
Jurassic
Basement
Slope fan deposit
Basin floor fan
ABSMA
Moho
Seismic (default)
8000.00
5000.00
4000.00
3000.00
2000.00
1000.00
0.00
-1000.00
-2000.00
-3000.00
-4000.00
-5000.00
0
10
20km
V.E.: 3:1
Geoex
Oceanic crust
Transitional crust
Continental crust

The crustal interpretation shown on Figure 7 is based on the geophysical cross-section from Klingelhoefer et al. (2009) (Figure 3) that crosses the southern part of the TDB offshore Dakhla and runs roughly parallel to the seismic line shown in Figure 7. Based on the interpretation by Klingelhoefer et al. (2009), the continental crust is located basinward of the WACMA (Figure 2) and is 40 km in width. The transitional crust has a blocky basement surface and extends over a width of 130 km. This transitional crust includes the ABSMA that is 35 km wide and marked by half-grabens filled with post-rift magmatic flows. The oceanic crust in the northwestern area has a smoother surface and extends over 60 km (Figures 1, 2).

4.2 Subsurface mapping of the Moroccan Middle Atlantic passive margin

4.2.1 Rifted basement geometry, subsidence, and total sedimentary thickness

Triassic-Early Jurassic rifting in the TDB formed a series of half-grabens in the Precambrian basement that were filled by syn-rift, Triassic sedimentary rocks (Von Rad and Einsele, 1980). Basement depth varies significantly from south to north (Figure 8.A) and records major subsidence in the northeastern part of the TDB as shown by excess sediment thickness (around 19 km). This area of the deeply subsided margin was previously named the Cape Boujdour Marginal Rift (Von Rad and Einsele, 1980). The elevated top basement in the southeastern part of the basin forms a seaward extension of the Precambrian Reguibat Shield that is exposed inland (Labails et al., 2009) (Figures 1, 2).

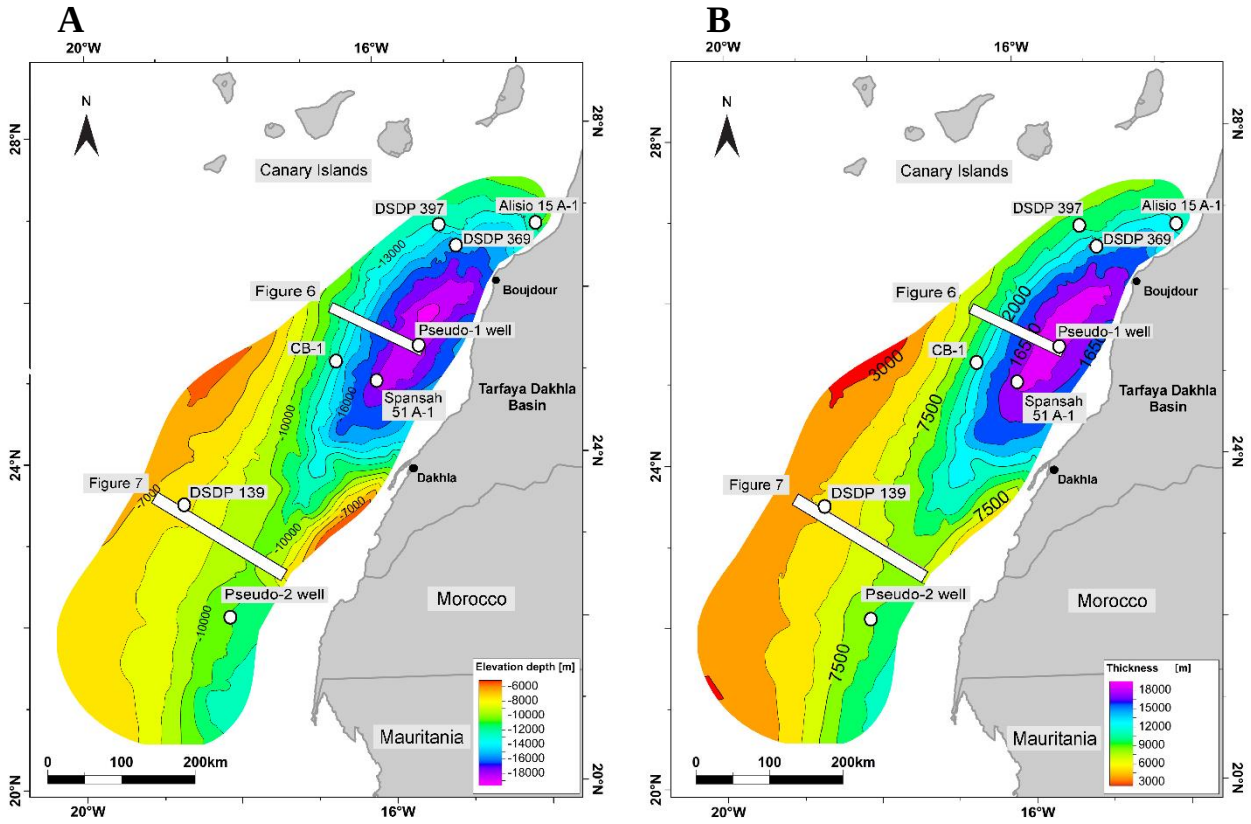

Figure 8: A. Top basement depth structure map showing the subsiding margin in the northeastern part of the basin at the Cape Boujdour marginal rift defined by Von Rad and Einsele (1980). The basement high in the eastern area is close to the WACMA from Klingelhoefer et al. (2009). **B.** Total sediments isopach map showing the thickness variation across the study area with the greatest sediment thickness along the northeastern part at the Cape Boujdour marginal rift and with the thickness decreasing in a southward direction.

The top basement surface is also elevated in the western part of the TDB along a broad basement arch that trends northeast between the Canary Islands in the north and Cape Verde in the south (Holik et al., 1991). This basement arch is also observed on the regional magnetic anomaly map (Figure 2). The origin and formation of this bulge are still debated but the presence of this bulge does not support the proposal by Patriat and Labails (2006) that the volcanic islands of the Canary and Cape Verde Islands developed from two separate hotspots rather than a single one (Patriat and Labails, 2006) (Figure 2).

Maximum sediment thickness in TDB is around 19 km in the northeastern part of the basin above the Cape Boujdour Marginal Rift, while its thickness decreases towards the elevated basement along the southeastern and southwestern margins of the basin with a 3 km minimum thickness (Figure 8.B).

4.2.2 Jurassic carbonate platform

During the Jurassic, transgression reached its peak during the Oxfordian-Kimmeridgian, when the siliciclastic sediment supply was low in the TDB. These conditions allowed the formation of a massive carbonate reef and platform complex (Hafid et al., 2008). Figure 9A shows that the width of the carbonate platform ranges from 20 km to a maximum width of 140 km.

Maximum Jurassic thickness in the TDB is 14 km and fills the subsiding basement sag of the Cape Boujdour Marginal Rift at the northeastern part of the basin (Figure 9.B). The Jurassic thickness decreases toward the western part of the TDB where the Jurassic onlaps the elevated basement area.

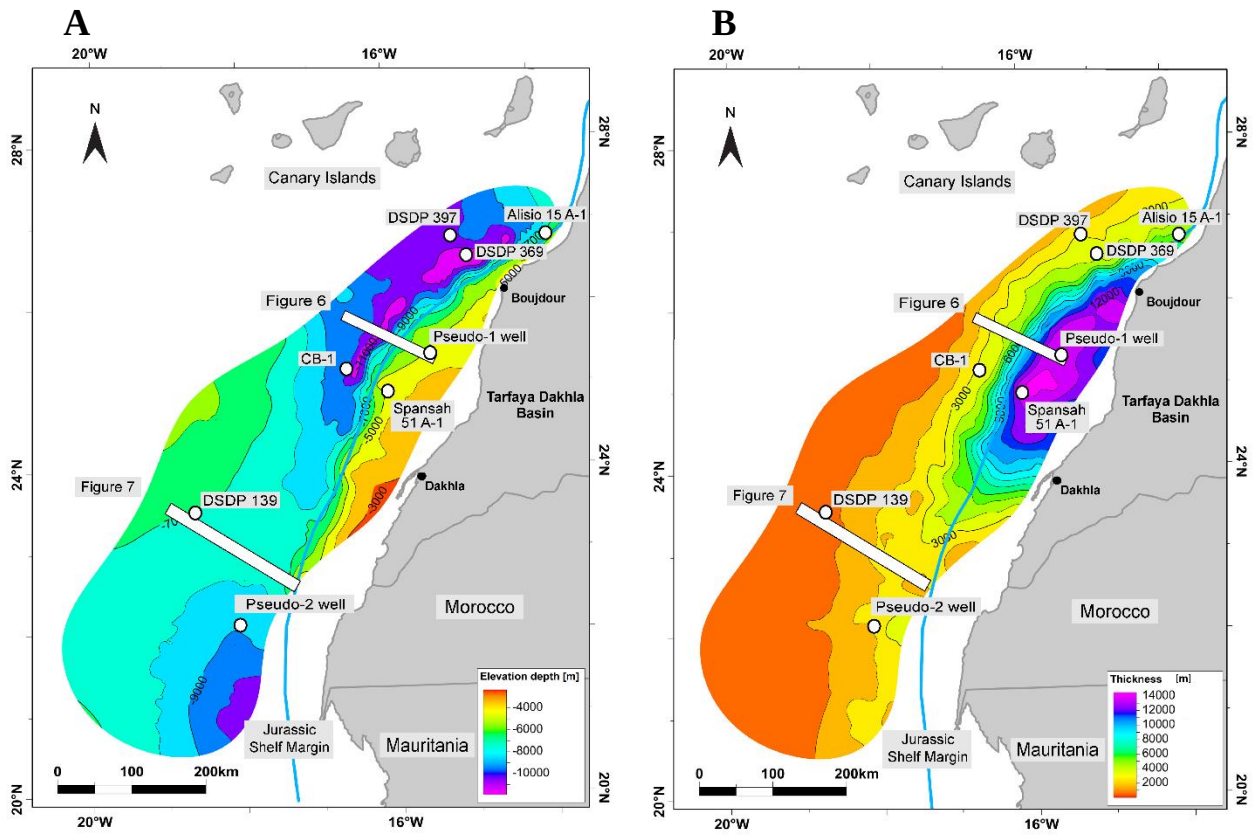

Figure 9: A. Top Jurassic depth structure map showing the extension of the carbonate platform in the eastern part of the Tarfaya Dakhla basin. The blue line delineates the extension of the Jurassic shelf margin **B.** Jurassic isopach map showing the increase in sediments thickness in the northeastern part of the study area where the Jurassic sediments filled the area of the proposed Cape Boujdour marginal rift (Von Rad and Einsele, 1980).

4.2.3 Mesozoic clastic sediment supply, delta formation, gravitational collapse, and passive margin formation

As a result of major sea-level regression and the increase in continental sediments supply in the Lower Cretaceous age, a 1-4 km thick section of continental-to-marine deltaic section was deposited on the shelf with submarine fans downdip in the distal basin (Shipboard Scientific Party, 1979; Von Rad and Einsele, 1980; ONHYM, 2019). High rates of clastic, deltaic sediment supply during the Cretaceous (Figure 1) led to over-steepening and gravitational collapse in the TDB, which formed a roll-over anticline and down-dip thrusts in the deeper part of the basin (Heyman, 1989; Nemcok et al., 2005; ONHYM, 2019).

The top Berriasian map reflects the main structural features in the TDB. The eastern part of the TDB is deformed by a zone of listric, normal faults with an updip, extensional zone, trending northeast-southwest, and extending over 480 km long and 30 km wide (Figure 10.A). The dip of these listric, normal faults increase with depth and sole out along a Jurassic detachment surface. The normal faults extend upward to the base Cenozoic which indicates these normal faults were active during this time (Figure 6).

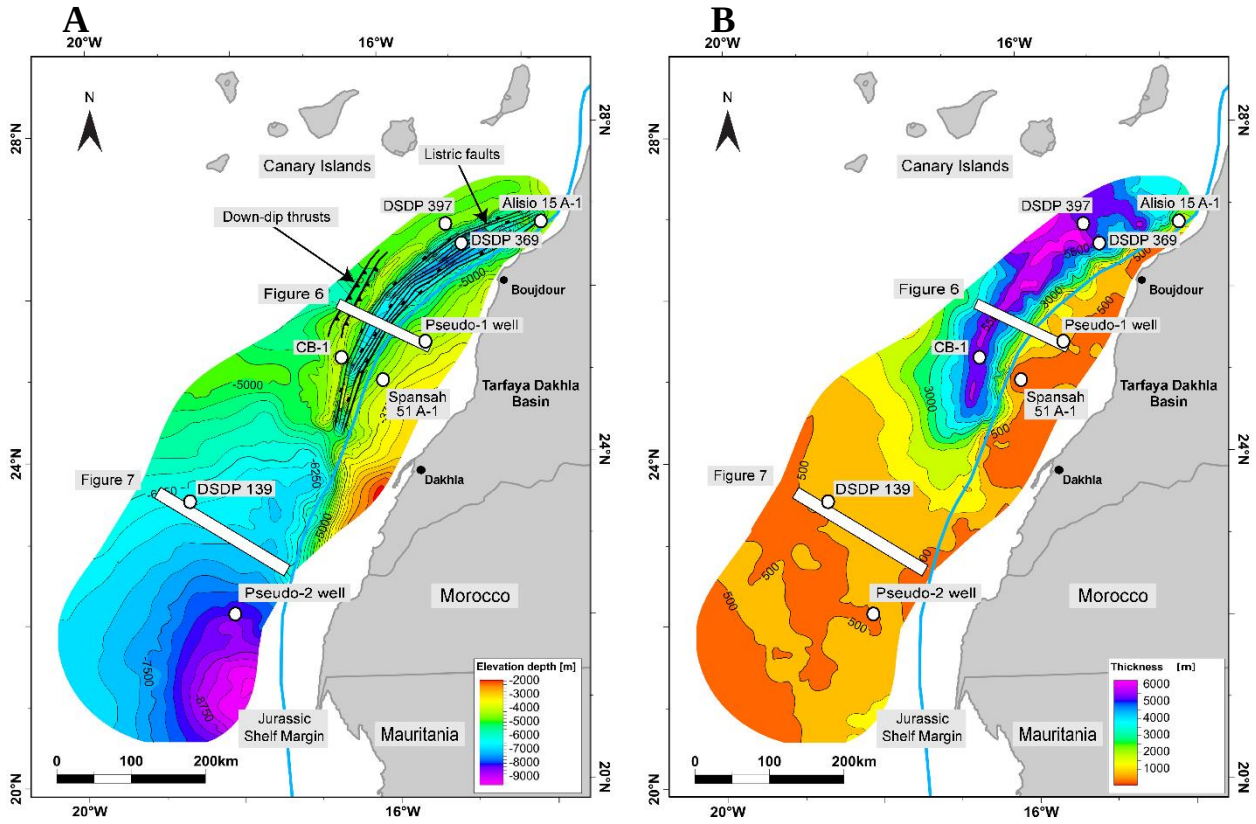

Figure 10: A. Top Berriasian depth structure map showing listric normal faults striking northeast-southwest within the updip extension zone of the passive margin fold belt. A roll-over anticline and compressional down-dip thrusts zone define the downdip part of the passive margin fold belt (PMFB). **B.** Berriasian isopach map showing an increase of sediment thickness within the Berriasian depocenter that is centered in the roll-over anticline.

The horizontal translation over the Jurassic detachment surface formed a down-dip a roll-over anticline that is parallel to the zone of listric, normal faults and a down-dip thrust zone. The down-dip thrust zone is 117 km long and 15 km wide (Figure 10.A). The rollover anticline is one of the main targets for hydrocarbon exploration in the TDB and was drilled by the CB-1 well in 2015 and encountered oil shows in the Lower Cretaceous reservoirs trapped in the closure of the roll-over anticline (Lawrence, 2019)

The maximum thickness of the Berriasian occurs on the down-thrown side of the listric, normal faults at the roll-over anticline. High sedimentation rates at the Berriasian time resulted in the progradation of sediments beyond the shelf margin and into the deeper Cretaceous depocenter in the northwestern part of the basin (Figure 10.B). Maximum Berriasian thickness is around 6 km over the depocenter and decreases to 500 m towards the southern and eastern parts of the TDB basin (Figure 10.B).

The top Lower Cretaceous map is similar to the Berriasian, but it exhibits fewer listric normal faults within the extensional zone, and the down-dip thrust zone is not expressed on this surface (Figure 11.A). The maximum thickness of the Lower Cretaceous sediments is around 9 km on the roll-over anticline and decreases towards the southern and eastern parts of the TDB basin (Figure 11.B).

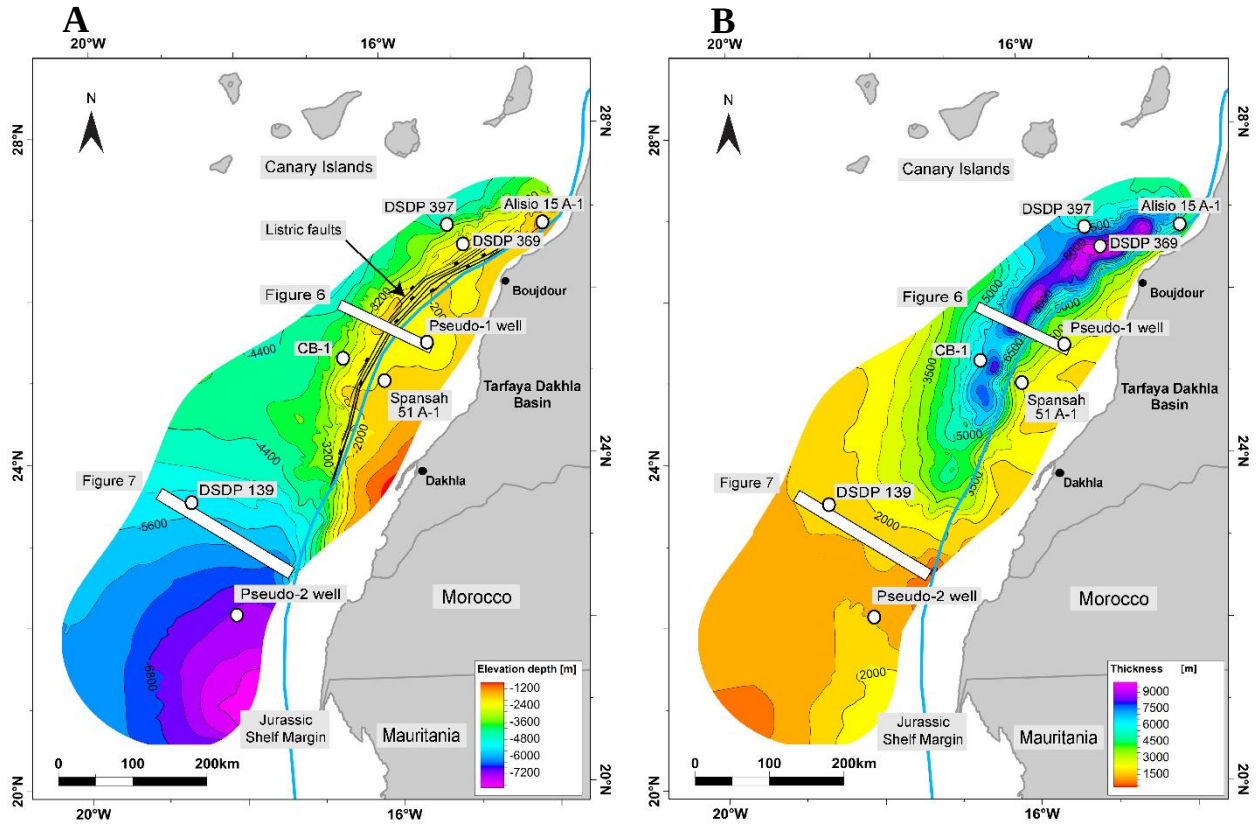

Figure 11: A. Top Lower Cretaceous depth structure map showing the zone of listric normal faults striking northeast-southwest parallel to the slope margin. The density of the listric normal faults is lower at the Lower Cretaceous level as compared to the Berriasian (Figure 10.A). The passive margin fold belt deformation does not extend to the Lower Cretaceous surface. **B.** Lower Cretaceous isopach map showing the maximum sediment thickness within the Lower Cretaceous depocenter in the area of the roll-over anticline. The Berriasian sediment thickness forms a major part of the total Lower Cretaceous thickness.

4.2.4 Upper Cretaceous slope front erosion

A major Oligocene, global regression along the Moroccan passive margin was synchronous with an increase in the Antarctic Bottom Water (AABW) flow. This regressive event triggered slumps, submarine canyons, and slope front erosion, that eroded 1400 m of sediments as deep as the Hauterivian in the DSDP 397 well in the northwestern part of the TDB (Arthur et al., 1979; Shipboard Scientific Party, 1979; von Rad and Wissmann, 1982).

The top Upper Cretaceous depth structure map shows a major slope front hiatus across the northwestern part of the TDB (Figure 12A). The black-dotted line through the Canary Islands represents the hot spot track through time (Neumaier et al., 2016). The top Upper Cretaceous is elevated in the eastern part of the basin and is deeper to the south.

The maximum thickness of the Upper Cretaceous occurs in the southeastern part of the TDB and represents a significant migration of the depocenter from the northeast at the Lower Cretaceous to the southwest at the Upper Cretaceous. The thickness of the Upper Cretaceous decreases towards the northwest direction (Figure 12B).

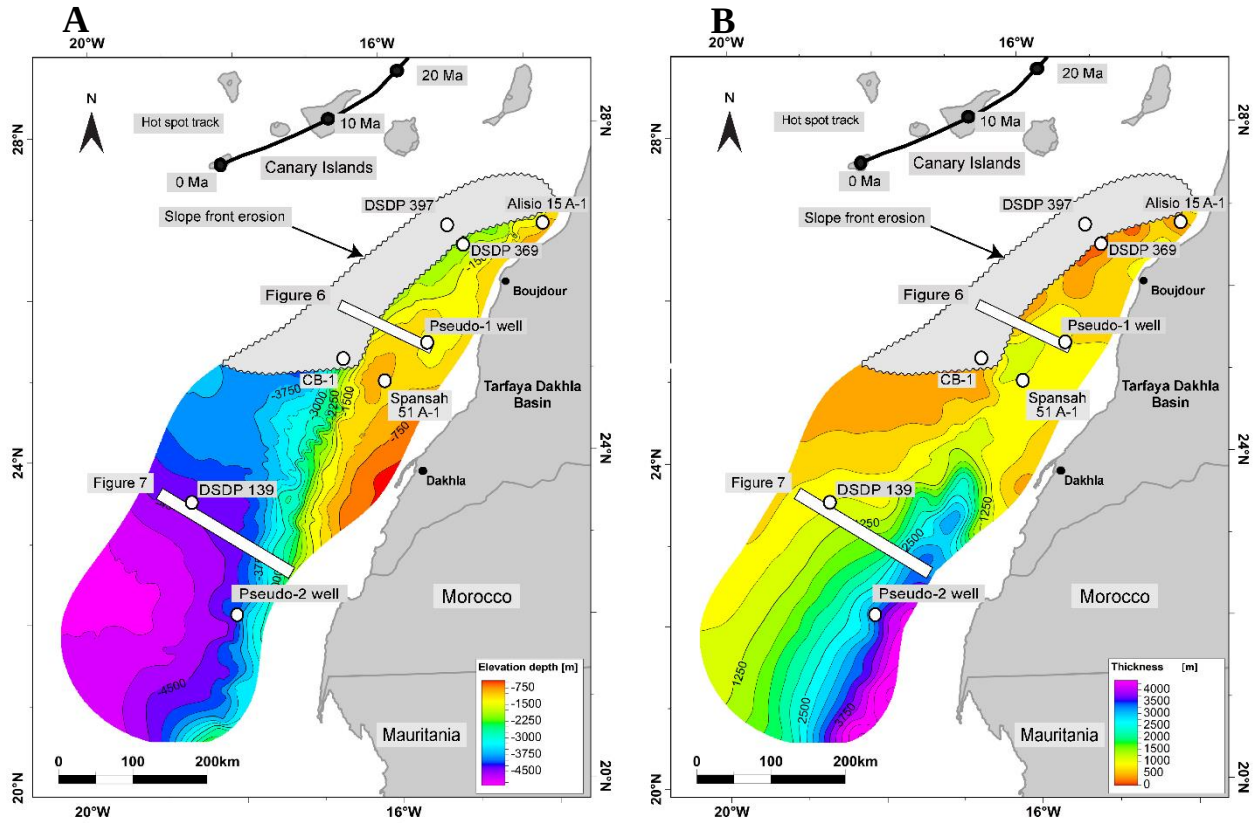

Figure 12: A. Top Upper Cretaceous depth structure map showing a major slope front erosion at the northwestern part of the basin as shown by the grey polygon. This erosion may have been related to a major Oligocene regression that was synchronous with an increase in the Antarctic Bottom Water (AABW). This period of lower sea level would have triggered slumps, submarine canyons, and slope front erosion that eroded as deeply as the Hauterivian as observed in the DSDP 397 well (Arthur et al., 1979; Shipboard Scientific Party, 1979; Von Rad and Wissmann, 1982). The black dotted line shows the 60-0 my, margin-parallel track of the Canary Islands hotspot. **B.** Upper Cretaceous isopach map showing the Upper Cretaceous depocenter is centered in the southern part of the basin at Pseudo-2 well. The Upper Cretaceous thickness decreases towards the northwest.

4.3 Estimation of the detachment depth using the area-depth-strain (ADS) analysis

Theory of ADS analysis. Chamberlin (1910) used bed length and displaced area measurements to estimate the detachment depth in a thrust belt. He observed that the structural relief area produced by compression is equal to the displaced area over the detachment. Epard and Groshong (1993) plotted the excess area as a function of depth to estimate both the detachment depth and the structural displacement parallel to the detachment where the pre-growth layers within the deformed section exhibit linear relation between fold area and depth. In contrast, the syn-deformation, growth layers show a decreasing trend upwards (Epard and Groshong Jr., 1993).

The term Layer Parallel Strain (LPS) was introduced by Groshong and Epard (1994) in their study of how bed lengths may deform during deformation by LPS within each formation. The power of the area-depth-strain analysis is that the estimated horizon displacement is based on the cross-sectional area that is conserved during the deformation (Groshong and Epard, 1994).

ADS application. In this study, I applied the Area-Depth-Strain (ADS) analysis using StructureSolver® software to estimate the horizons displacement, detachment dip, and depth of the regional Jurassic detachment. I applied the ADS analysis to the down-dip thrust zone and to the updip extensional zone of the passive margin foldbelt.

4.3.1 Application of ADS at the down-dip thrusts zone of the PMFB

I applied ADS analysis to measure the depth to detachment at the down-dip thrusts zone of the passive margin fold belt, as shown on the line in Figure 13. The solid yellow vertical axis represents the depth values, while the colored squares represent the folded area value within each layer. The best-fit line indicates a general increase in the folded area upwards through the pre-growth layers (from layer 1 to Valanginian). There is no decreasing trend in area within the upper layers.

The deflection point between the increase and decrease in fold area is missing, which indicates that the growth strata are absent. The inverse of the slope of the best-fit line gives the best-fit displacement, which equals -1070 m. In Figure 13, the values between brackets represent the specific nominal displacement and the LPS for each layer. The depth of the interpreted detachment is ± 9,900 m, while the best-fit detachment depth is ±10,300 m. This discrepancy may reflect the loss of area within the shaly, ductile layers due to thickening, which would violate the conservation of area concept used in the ADS analysis.

A more detailed interpretation of the best-fit line shows that there could be three separate, shorter, best-fit trends. These trends are between; **A-** Jurassic and layer 2, **B-** Layer 3 and layer 7, and **C-** Berriasian to Valanginian. These three trends may indicate the presence of three parallel detachments within a broader detachment zone - rather than a single, narrow detachment. This interpretation also validates the presence of the interpreted, shallower detachment (Figure 13).

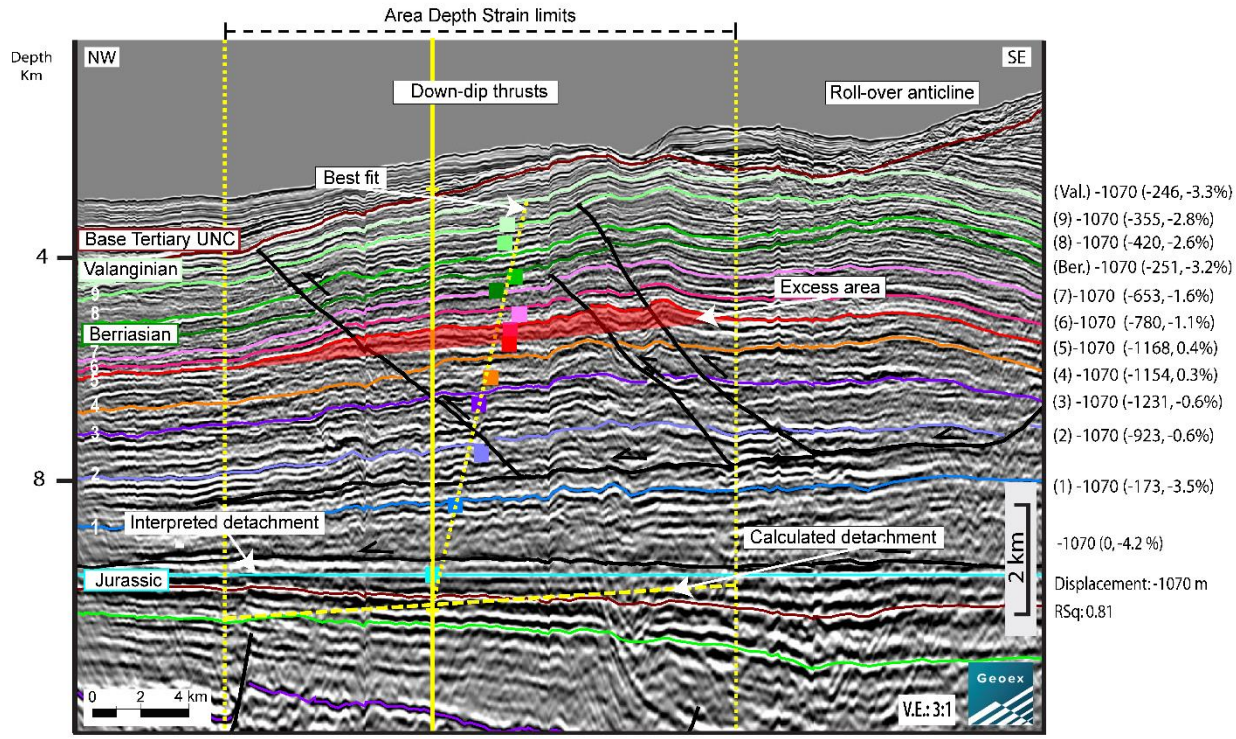

Figure 13: Application of area-depth-strain analysis (ADS) to measure the deeply buried, depth to detachment beneath the down-dip thrusts zone. The solid yellow vertical axis represents the depth, and the colored squares represent the excess area values at each layer. The ADS analysis indicates a general increase in excess area upwards through the pre-growth layers (that include the zone from Layer 1 to the Valanginian). There is no decreasing trend at the upper layers, which indicates the absence of growth strata during this period. Based on ADS, the interpreted depth to detachment is ± 9900 m, while the best-fit detachment depth is ± 10300 m. This predicted zone of detachment may reflect the loss of area at the shaly, ductile layers due to thickening, which violates the ADS analysis that is based solely on the conservation of area. More detailed interpretation of the best-fit line shows that the possibility of three, smaller, best-fit lines indicative of a zone of three detachments rather than a single detachment: 1) From Jurassic to layer 2, 2) From layer 3 to layer 7, and 3) from Berriasian to Valanginian. Values at each layer include: 1) best-fit displacement, 2) nominal displacement, and 3) layer parallel strain.

4.3.2 Applying ADS at the regional extension and compression zones of the PMFB

Application of the ADS analysis on a regional scale is based on linking the total, up-dip extension along the listric normal faults to the down-dip, compression associated with the roll-over anticline, and the down-dip thrusts. The ADS analysis can estimate the net displacement as previously shown for the Mexican Ridges passive margin fold belt in the western Gulf of Mexico by Eichelberger et al., (2017), who set the ADS limits along the two flat boundaries of the passive margin foldbelt.

Figure 14 shows ADS results for the shaded area under the Berriasian datum that represents the extension as a positive value. In contrast, the shaded area above the datum represents the compression shown as a negative value. The net displacement from the best-fit line is -3869 m, which indicates that the system has more compression than extension and could suggest the presence of an unrecognized, deeper folding mechanism. Values at each layer include the best-fit displacement, the nominal displacement, and the layer-parallel strain (LPS). The depth of the best-fit detachment matches the interpreted detachment seen on the seismic line at a depth of ± 9900 m.

Figure 14: Application of area-depth-strain analysis (ADS) to estimate the detachment depth based on the regional extension and compression of the passive margin fold belt. The colored squares represent the excess area value for each horizon. The shaded area under the regional datum at the Berriasian horizon represents the extension in positive values, while the compression above the datum is shown as negative values. The net displacement from the best-fit line is -3869 m, which indicates that the system exhibits more compression than extension that may reflect a deeper folding mechanism. Values at each layer include: 1) best-fit displacement, 2) nominal displacement, and 3) layer parallel strain. The depth of the best fit detachment is similar to the interpreted detachment at ± 9900 m.

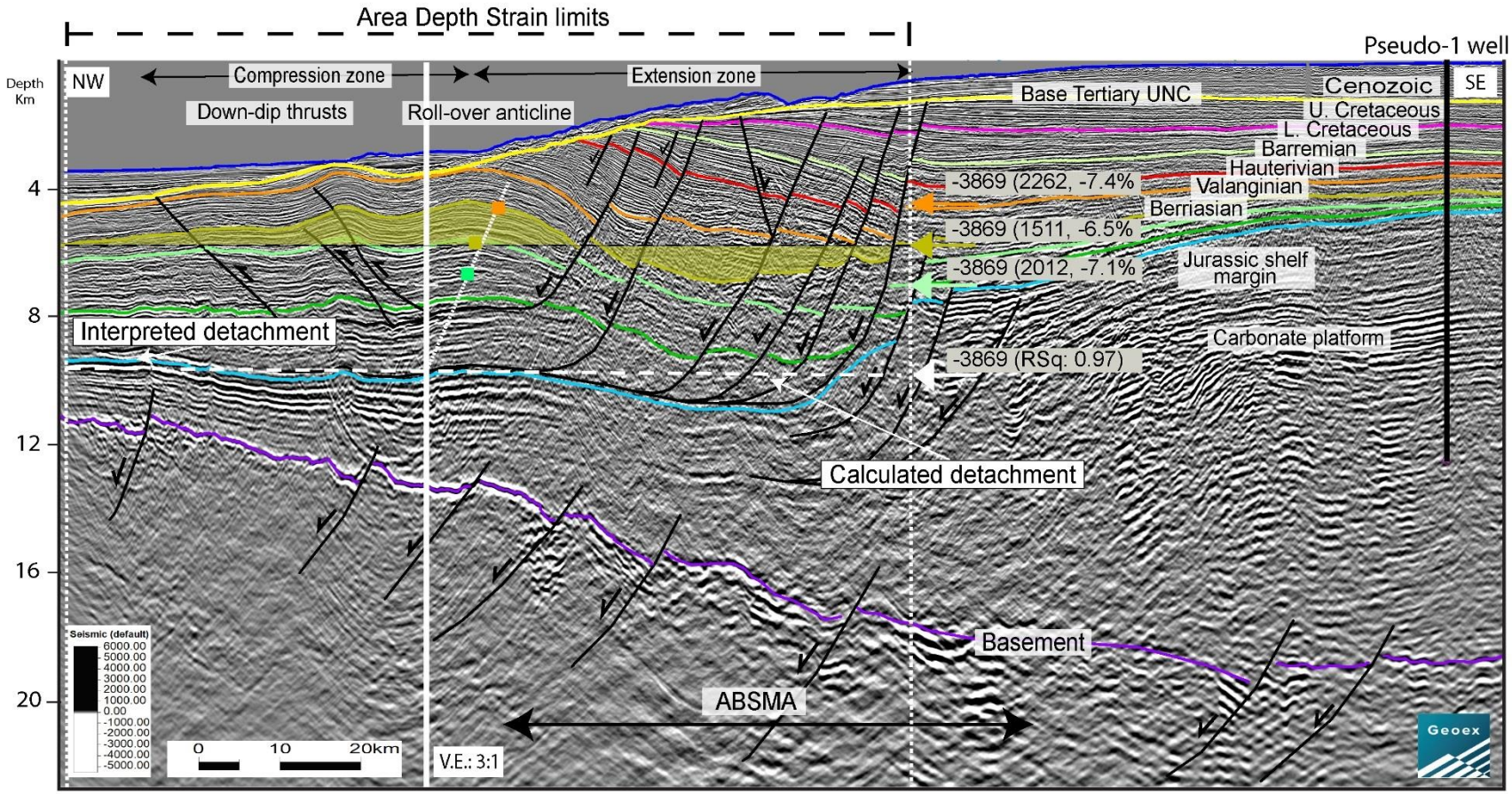
Area Depth Strain limits
Pseudo-1 well
Depth Km
NW
SE
Compression zone
Extension zone
Down-dip thrusts
Roll-over anticline
Base Tertiary UNC
Cenozoic
U. Cretaceous
L. Cretaceous
Barremian
Hauterivian
Valanginian
Berriasian
Jurassic shelf margin
Carbonate platform
-3869 (2262, -7.4%
-3869 (1511, -6.5%
-3869 (2012, -7.1%
-3869 (RSq: 0.97)
Interpreted detachment
Calculated detachment
Basement
ABSMA
4
8
12
16
20
Seismic (default)
6000.00
5000.00
4000.00
3000.00
2000.00
1000.00
0.00
-1000.00
-2000.00
-3000.00
-4000.00
-5000.00
0
10
20km
V.E.: 3:1
Geoex

4.4 Basin modeling at the Tarfaya Dakhla basin

4.4.1 Data used for basin modeling

Early exploration activities in the Moroccan Atlantic margin included the drilling expeditions of the Deep Sea Drilling Project (DSDP), which were carried out during the 1970s. DSDP work included the drilling of DSDP wells 397, 369, and 139 in the offshore TDB (Figure 2).

These DSDP wells penetrated and partially cored the Cenozoic, Upper Cretaceous, and Lower Cretaceous section to study their depositional environment, stratigraphy, petroleum geochemistry, and the physical properties of the sedimentary rocks (Hayes et al., 1972; Shipboard Scientific Party, 1978). Little information is available from the published literature about the source rock properties from the exploratory wells by the oil industry within the TDB (Lawrence, 2019; ONHYM, 2019).

DSDP well 369. This well penetrated a continuous section of the Neogene, the Oligocene, and part of the Upper Cretaceous. Minor unconformities were observed at several intervals, but the most significant unconformity is the hiatus between the Coniacian and middle to lower Albian, which was attributed by the Shipboard scientific Party (1978) to slumping (Figure 4). Measured Total Organic Carbon (TOC) is 2.3% at a depth of 2195 m in the Albian, and vitrinite reflectance values show a wide range between 0.13-0.31 % (Kendrick et al., 1978).

A recent geochemical study in DSDP 369 well by (Cool et al., 2008) showed that the Albian-Campanian source rock has more hydrocarbon potential than reported previously by the

Shipboard Party (1978). Samples selection by Cool et al. (2008) focused more on the darker core samples with higher-organic content, which are usually associated with higher hydrocarbon potentiality. TOC values in the new samples range from 0.42 to 11.53%, which is higher than the values stated by Kendrick et al., (1978).

Organic matter in DSDP 369 is mainly oil-prone, Type-2 kerogen with minor gas-prone Type-3 kerogen. These organic-rich rocks correlate with organic-rich units deposited during Cretaceous Oceanic Anoxic Events (OAEs): 1) the Early to mid-Albian section correlates with the OAE-1B event; 2) the Late Albian-Early Cenomanian section correlates with the OAE-1D event, and 3) the Cenomanian-Turonian section correlates with the OAE2 event. Some samples show high generation potential values (>2.5 mg HC/g rock), which indicates these rock could generate sufficient hydrocarbons if they reached higher maturity levels (Cool et al., 2008).

DSDP well 397. This well encountered hydrocarbon gases generated in situ by lower-temperature digenetic processes. TOC values range from 0.4 to 3.4 %, while measured vitrinite reflectance values range from 0.16 to 0.49 %. These observations indicate that source rocks in DSDP well 397 are generally immature but act as a potentially mature source rock if buried 1500 to 2000 m deeper (Shipboard Scientific Party, 1979).

Evidence of potential deeper Jurassic and Lower Cretaceous mature source rocks is provided by the hydrocarbons encountered from the Jurassic carbonates along the TDB, which likely migrated upward from deeper, mature source rocks as observed at the exploratory wells; Spansah 51 A-1, Alisio 15 A-1, and the CB-1 wells (Lawrence, 2019; ONHYM, 2019) (Figure 5).

The exploratory well CB-1 drilled in the southern offshore Boujdour area in 2015 encountered gas and liquid hydrocarbons trapped in a large, roll-over anticline. These hydrocarbons indicate possible kitchen for Jurassic and Lower Cretaceous source rocks that were deposited above the Mesozoic oceanic crust of the Central Atlantic (ONHYM, 2019) (Figure 2).

4.4.2 Vitrinite reflectance and total organic carbon content of potential source rocks

The offshore TDB has as many as five potential source rock units that include: the Jurassic, the Valanginian-Barremian, the Aptian-Albian, the Cenomanian-Turonian, and the Campanian (Gesamtfakult et al., 2014; Sachse et al., 2016; ONHYM, 2019) (Figure 4).

Jurassic source rocks of the TDB shelf and slope areas. Since the Jurassic source rocks of the TDB are associated with the oceanographic turnover during the Toarcian, their TOC values and maturity vary according to their location within the TDB:

1) **In the shelf area of the TDB:** TOC values of the Lower Jurassic are low and range between (0.1-0.3 %). TOC values of the Middle Jurassic, Callovian, and Oxfordian source rocks vary between 1.47-2.49 % (Gesamtfakult et al., 2014). TOC values of the Upper Jurassic, Kimmeridgian vary between 0.2-0.5 %. In the Pseudo-1 well at the shelf, I used 2 %TOC and 300 mg HC/g TOC HI for modeling the middle Jurassic.
2) **In the slope area of the TDB:** Jurassic carbonates are more shaly, and the TOC values in the Lower Jurassic are between 0.42-8.89 %. The hydrogen index value is 550 mgHC/g TOC. Jurassic source rocks are mainly, Type 2 kerogen with minor Type 1

kerogen (Gesamtfakult et al., 2014). I used values of 4% TOC, and 550 mg HC/g TOC HI for modeling the DSDP 397 and 369 wells, and the Pseudo-2 well.

Cretaceous source rocks of the TDB. Lower Cretaceous source rocks of the TDB are negatively impacted by the high sediment supply of the Tantan and Boujdour deltas (Figures 1, 2), which resulted in the dilution of their organic contents with consequent reduction of their TOC values (Gesamtfakult et al., 2014).

Hauterivian source rocks have TOC values around 0.5 % at the shelf and around 1% at the DSDP 397. The organic matter is mainly terrestrial, Type-3 kerogen (Gesamtfakult et al., 2014). For modeling, I used 1 % TOC in the DSDP 397, 369 wells and for the Pseudo-2 well models, and 200 mg HC/g TOC HI. In the Pseudo-1 well model, I used 0.5 % TOC and a HI of 200 mg HC/g TOC.

Albian source rocks are mainly marl and shale that were deposited during the oceanic anoxic events (Sachse et al., 2016). HI values range between 400-700 mgHC/g TOC, while TOC values are between (0.8- 4 %) at the shelf and increase to 6% at the slope in the DSDP 369 well. To generate the models, I used 4% TOC in the DSDP 369 and Pseudo-2 well models and 380 mg HC/g TOC for HI. In the Pseudo-1 well model, I used 3 % TOC and 380 mg HC/g TOC for HI.

Campanian source rocks are rich in calcareous nanoplanktons, dispersed biogenic silica, planktonic foraminifera as described by Sachse et al., (2011). The organic matter is mainly Type-2 with an average TOC value of 4.5 %, and a HI of 650 mgHC/g TOC. To build the models, I used a 4 % TOC value and HI of 600 mg HC/g TOC for Pseudo-1 well and Pseudo-2 well models.

4.4.3 Basin model boundary conditions

Sediment-water interface temperature values (SWIT) were calculated using PetroMod® software based on the equations by Wygrala, (1989). PetroMod® software uses the latitude, longitude, and the current surface temperature to estimate the paleo-mean surface temperature and make corrections for the paleo-latitude and paleo-depth through time.

Paleo-water depth was directly estimated from seismic, formation tops, and basin history. Heat flow values were estimated based on the values in rifted margins stated by (Hasterok, 2013), and the published heat flow maps by (Hyndman et al., 1987). The heat flow values at the rifting phase are at their highest level of 65 mW/m^2, then decrease gradually through time to a value of 42 mW/m^2.

The heat flow values reach their highest temperature at the Pseudo-1 well model on the shelf where the conductivity of rocks is high, and the surface water temperature is higher than the other locations (19 ºC compared to 5ºC at the deeper models). The maximum heat flow value is 75 mW/m^2 at the rifting phase and decreases gradually to 50 mW/m^2 at the surface.

4.4.4 Basin modeling results

In order to evaluate the source rock potentiality of the Jurassic, Lower Cretaceous, and Upper Cretaceous in the TDB**,** I created four basin models using PetroMod® software under different physiographic locations: 1) DSDP 397 located on the uppermost rise; 2) DSDP 369 located on the slope; 3) Pseudo-1 well located on the shelf; and 4) Pseudo-2 well located within the thickest Upper Cretaceous depocenter (Figure 2).

I used measured temperature, and vitrinite reflectance (Ro) values from the DSDP 397 well to calibrate the generated model. Figure 15.A shows the calculated vitrinite reflectance using the Easy% Ro method by Sweeney and Burnham (1990) that is compared to the measured Ro values in the DSDP 397 well. Measured Ro values range from 0.16 to 0.49 % and generally correlates with the modeled values. Both Ro trends show a deflection at 4207 m at the top Hauterivian unconformity that resulted from the slope front erosion at this level.

Four temperature points were recorded in DSDP 397 well represented by white triangles shown in Figure 15 B. The sea bottom temperature is 4.75 ºC at 2910 m and underlain by three points of 19.5 ºC at 3271 m; 22.5 ºC at 3358 m; and 24 ºC, at 4348 m. A straight line passing through the seafloor, the second, and the third points will give a thermal gradient of 4.2 ºC/100 m. This high thermal gradient may reflect the proximity of the Canary Islands hotspot track during the mid-Cenozoic (Figures 1, 2).

There is an overall correlation between modeled and measured temperature values except at the fourth point that has a lower temperature (Figure 15.B). This shift in temperature may be the result of excess circulation at this location (Shipboard Scientific Party, 1979).

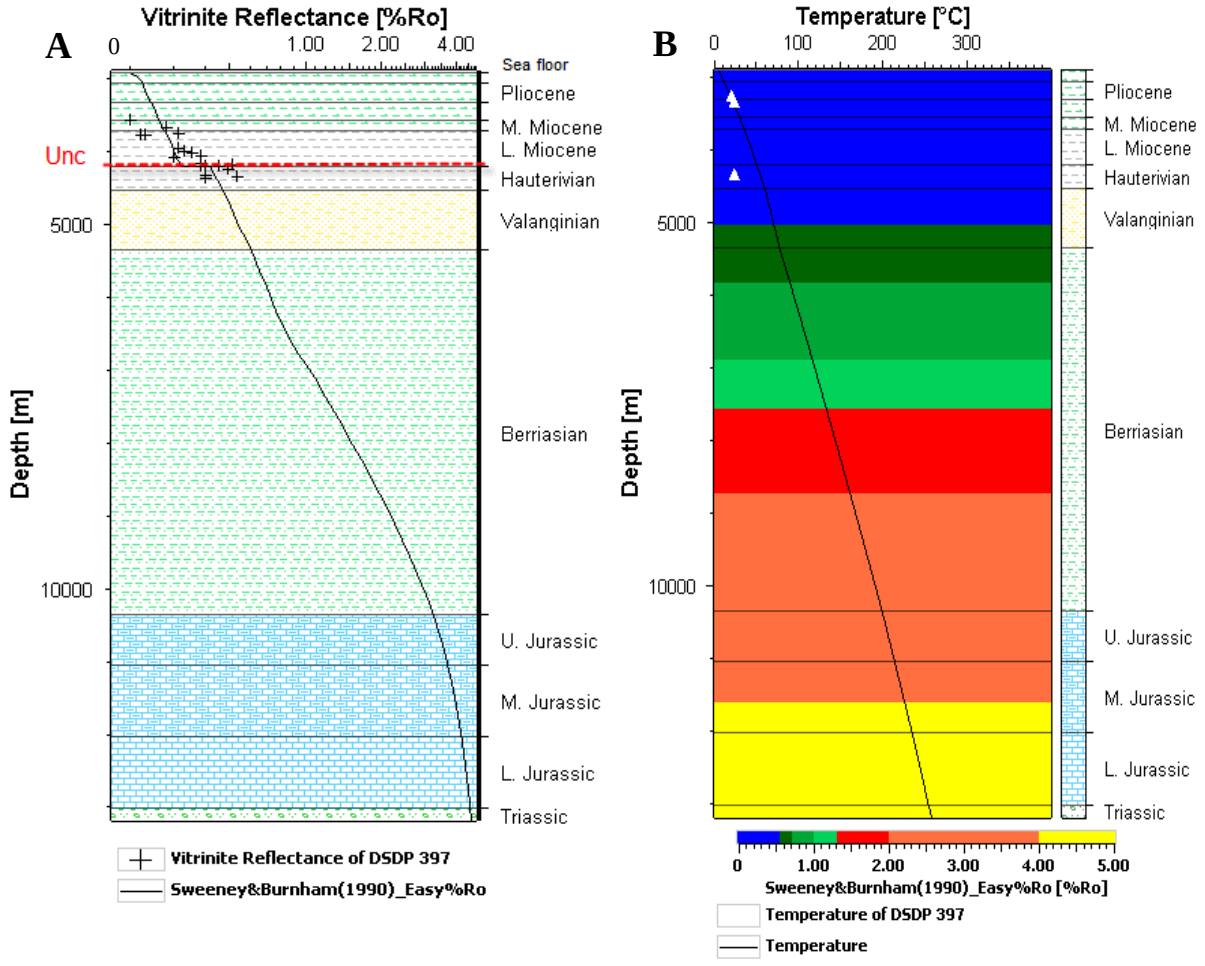

Figure 15: A. Modeled versus measured vitrinite reflectance in DSDP 397 well showing the deflection at the top Hauterivian unconformity at 4207 m that is produced by 1400 m of late Cretaceous slope front erosion. **B.** Modeled versus measured temperature values with modeled vitrinite reflectance overlay. (**Blue color** = immature; **green color** = oil window; **red color** = gas window; and **yellow color**= over-mature). Potential Hauterivian source rocks have been documented from core samples to be immature in the DSDP 397 well.

Burial history of the DSDP 397, 369, Pseudo-1 well, and Pseudo-2 well basin modeling sites in (Figure 16) reveals the following observations and conclusions:

1) The maximum subsidence rate is from 150 to 130 Ma at the DSDP 397 and 369 wells, while the Pseudo-1 well model has a higher subsidence rate in the period from 210 to 135 Ma.
2) High subsidence rates are due to the flexural subsidence in the area of the Cape Boujdour marginal rift (about 6-7.5 km) that are related to the underlying rift structure and/or the overlying mass of the Jurassic carbonate build-up (Von Rad and Einsele, 1980).
3) The Pseudo-2 well reveals a low subsidence rate along the southern part of the TDB without a significant subsidence of the basement (Figure 8.A).
4) The modeled transformation ratio indicates that that the Jurassic source rocks generated hydrocarbons at the Lower Cretaceous during the period of high subsidence rates; Jurassic source rocks are presently overmature in the TDB.
5) A potential Hauterivian source is currently in a late generative stage in the Pseudo-1 well and Pseudo-2 wells. The Albian source rocks are within the late generative stage only at the Psuedo-2 site. The Campanian source rocks are generally immature.

Figure 16: Burial history versus transformation ratio for the basin modeling sites at DSDP well 397, at DSDP well 369, Pseudo-1, and at Pseudo-2 modeling sites. **A.** The maximum subsidence rate occurred between 150 to 130 Ma at the DSDP 397 well. **B.** The maximum subsidence rate occurred between 150 to 130 Ma at the DSDP 369 well and is similar to the period of maximum subsidence at the DSDP 397 well. **C.** The highest, modeled subsidence rate occurred between 210-135 Ma at the Pseudo-1 well modeling site. **D.** The subsidence rate observed at the Pseudo-2 well modeling site is lower than the other sites. The modeled transformation ratio indicates that Jurassic source rocks generated hydrocarbons early but are presently overmature in the Tarfaya Dakhla basin. A potential Hauterivian source is currently within its late generative stage at the Pseudo-1 and Pseudo-2 modeling sites. The Albian source rocks are only within the late generative stage at the Psuedo-2 well modeling site. The Campanian source rocks are generally immature.

A

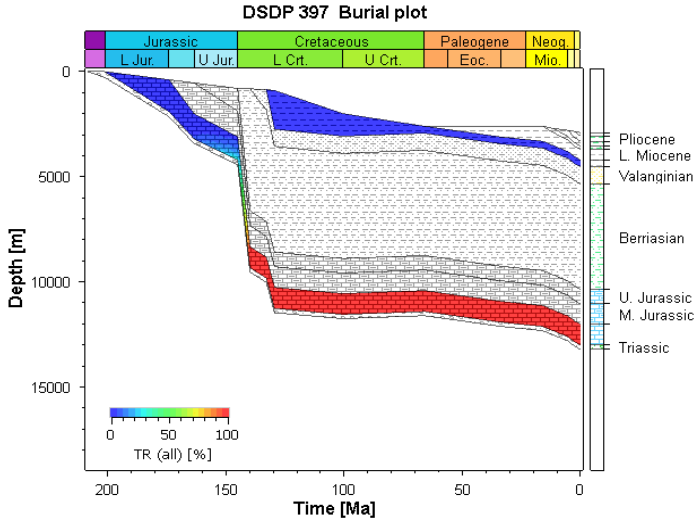
DSDP 397 Burial plot
Jurassic
Cretaceous
Paleogene
Neog.
L Jur.
U Jur.
L Crt.
U Crt.
Eoc.
Mio.
Depth [m]
0
5000
10000
15000
0
50
100
TR (all) [%]
200
150
100
50
0
Time [Ma]
Pliocene
L. Miocene
Valanginian
Berriasian
U. Jurassic
M. Jurassic
Triassic

B

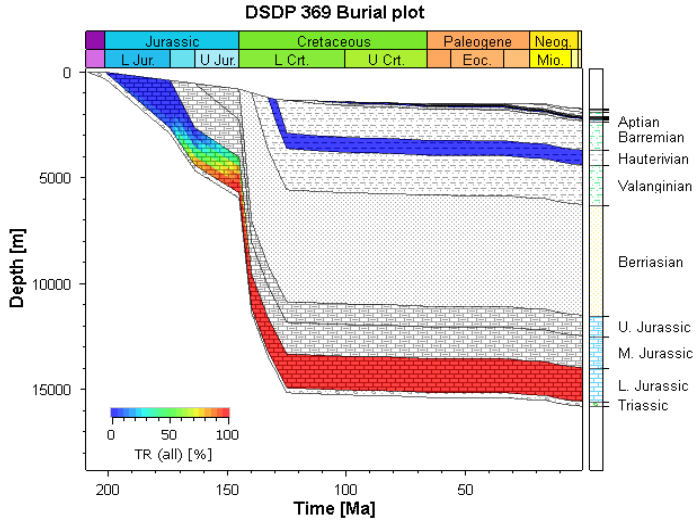
DSDP 369 Burial plot
Jurassic
Cretaceous
Paleogene
Neog.
L Jur.
U Jur.
L Crt.
U Crt.
Eoc.
Mio.
Depth [m]
0
5000
10000
15000
0
50
100
TR (all) [%]
200
150
100
50
Time [Ma]
Aptian
Barremian
Hauterivian
Valanginian
Berriasian
U. Jurassic
M. Jurassic
L. Jurassic
Triassic

C

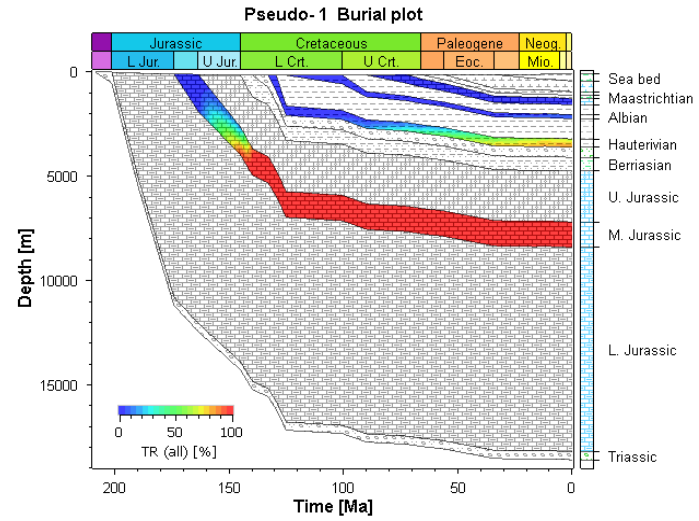
Pseudo-1 Burial plot
Jurassic
Cretaceous
Paleogene
Neog.
L Jur.
U Jur.
L Crt.
U Crt.
Eoc.
Mio.
Depth [m]
0
5000
10000
15000
0
50
100
TR (all) [%]
200
150
100
50
0
Time [Ma]
Sea bed
Maastrichtian
Albian
Hauterivian
Berriasian
U. Jurassic
M. Jurassic
L. Jurassic
Triassic

D

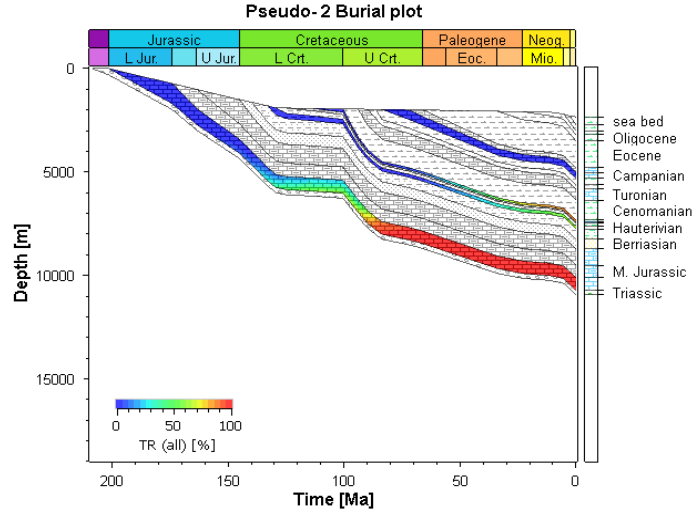
Pseudo-2 Burial plot
Jurassic
Cretaceous
Paleogene
Neog.
L Jur.
U Jur.
L Crt.
U Crt.
Eoc.
Mio.
Depth [m]
0
5000
10000
15000
0
50
100
TR (all) [%]
200
150
100
50
0
Time [Ma]
sea bed
Oligocene
Eocene
Campanian
Turonian
Cenomanian
Hauterivian
Berriasian
M. Jurassic
Triassic

Evaluating the vitrinite reflectance and transformation ratio versus time for the middle section of the Middle Jurassic at the Pseudo-1 well and the middle section of the Lower Jurassic at the DSDP 397, 369, and Pseudo-2 well basin models in (Figure 17), reveals the following observations and conclusions:

1) The hydrocarbon generation of the Lower Jurassic occurs between 170-140 Ma at the DSDP 397 and DSDP 369 wells and peaks to 98 % from 140 Ma to the present-day.
2) Hydrocarbon generation of the Lower Jurassic occurs between 140-80 Ma at the Pseudo-2 well and peaks to 95 % from 80 Ma to the present-day.
3) Hydrocarbon generation of the middle Jurassic at the Pseudo-1 model occurs between 160-145 Ma. All modeled sites are currently overmature (Ro>2.0).
4) These modeling results match the results of (Sachse et al., 2016) in the northern part of the TDB, where these authors noted that the Jurassic is the most mature source rock in the basin.
5) Figure 18 shows the vitrinite reflectance and transformation ratio versus time of the Hauterivian source rock at DSDP 397, 369, Pseudo-1 well, and Pseudo-2 well. There has been no significant maturation and generation at the DSDP 397 and 369 wells as they are not buried deeply enough.
6) The potential Hauterivian source is currently generative in both the Pseudo-1 well and Pseudo-2 well modeling sites and is within the gas window. Generation begins at the Upper Cretaceous in Pseudo-1 well modeling site, and at the Paleocene in Pseudo-2 well modeling site.

Figure 17: Vitrinite reflectance and transformation ratio versus time for the middle section of the Middle Jurassic at the Pseudo-1 modeling site and the middle section of the Lower Jurassic at the DSDP 397 well, at the DSDP 369 well, and at the Pseudo-2 modeling sites. **A.** Hydrocarbon generation of the Lower Jurassic occurred between 170-140 Ma at DSDP well 397. **B.** Hydrocarbon generation of the Lower Jurassic at the DSDP 369 well occurred between 170-140 Ma. **C.** Hydrocarbon generation of the middle Jurassic at the Pseudo-1 model occurred between 160-145 Ma. **D.** Hydrocarbon generation of the Lower Jurassic at the Pseudo-2 model occurred between 140-80 Ma. Jurassic source rocks are currently overmature (Ro>2.0) at the four modeling sites: DSDP well 397, DSDP 369, Pseudo-1 well, and Pseudo-2 well modeling sites.

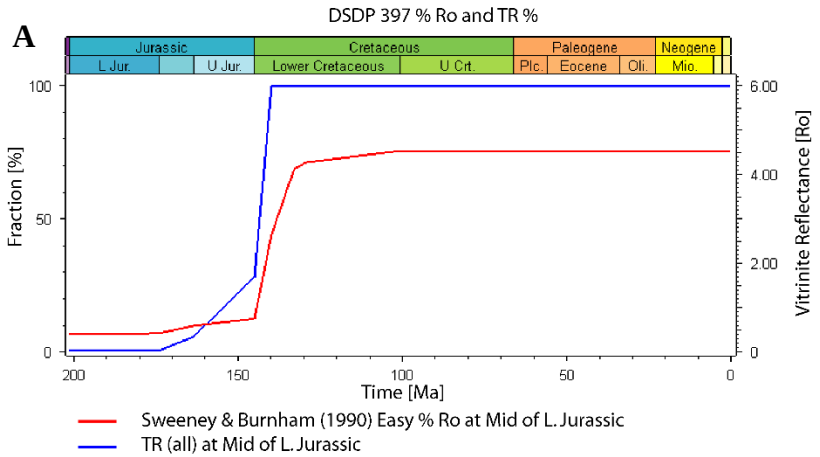
A
DSDP 397 % Ro and TR %
Jurassic
Cretaceous
Paleogene
Neogene
L Jur.
U Jur.
Lower Cretaceous
U Crt.
Plc.
Eocene
Oli.
Mio.
Fraction [%]
Vitrinite Reflectance [Ro]
Time [Ma]
Sweeney & Burnham (1990) Easy % Ro at Mid of L. Jurassic
TR (all) at Mid of L. Jurassic

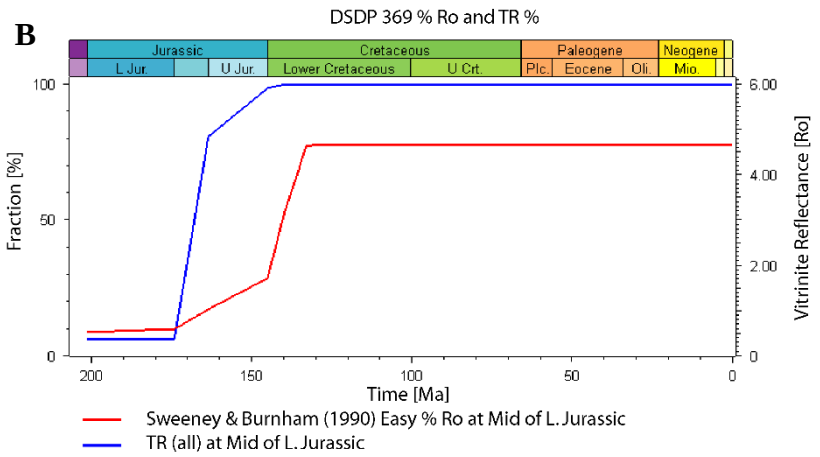
B
DSDP 369 % Ro and TR %
Jurassic
Cretaceous
Paleogene
Neogene
L Jur.
U Jur.
Lower Cretaceous
U Crt.
Plc.
Eocene
Oli.
Mio.
Fraction [%]
Vitrinite Reflectance [Ro]
Time [Ma]
Sweeney & Burnham (1990) Easy % Ro at Mid of L. Jurassic
TR (all) at Mid of L. Jurassic

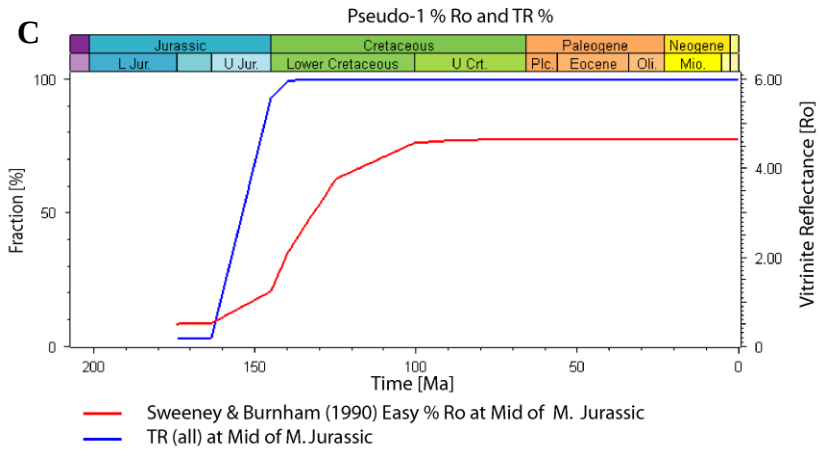
C
Pseudo-1 % Ro and TR %
Jurassic
Cretaceous
Paleogene
Neogene
L Jur.
U Jur.
Lower Cretaceous
U Crt.
Plc.
Eocene
Oli.
Mio.
Fraction [%]
Vitrinite Reflectance [Ro]
Time [Ma]
Sweeney & Burnham (1990) Easy % Ro at Mid of M. Jurassic
TR (all) at Mid of M. Jurassic

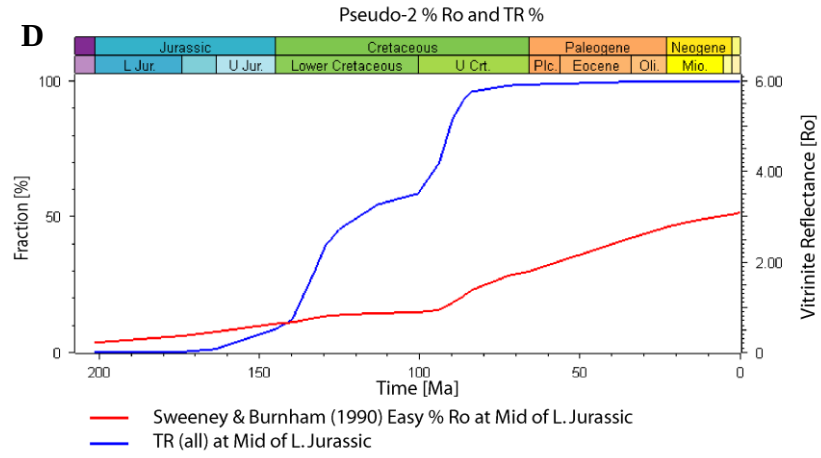
D
Pseudo-2 % Ro and TR %
Jurassic
Cretaceous
Paleogene
Neogene
L Jur.
U Jur.
Lower Cretaceous
U Crt.
Plc.
Eocene
Oli.
Mio.
Fraction [%]
Vitrinite Reflectance [Ro]
Time [Ma]
Sweeney & Burnham (1990) Easy % Ro at Mid of L. Jurassic
TR (all) at Mid of L. Jurassic

Figure 18: Vitrinite reflectance and transformation ratio versus time of the Hauterivian section at the modeling sites of DSDP well 397, DSDP well 369, Pseudo-1 well, and Pseudo-2 well. **A.** Modeling results at the DSDP 397 well show that there is no significant maturation and generation. **B.** Modeling results at the DSDP 369 well show that there is no considerable maturation and generation as was also modeled at the DSDP 397 well. **C.** Modeling results at the Pseudo-1 model show that the potential Hauterivian source is currently generative and within the gas window with generation having begun during the Upper Cretaceous. **D.** Modeling results at the Pseudo-2 model show that the potential Hauterivian source is currently generative and within the gas window. Generation began during the Paleocene.

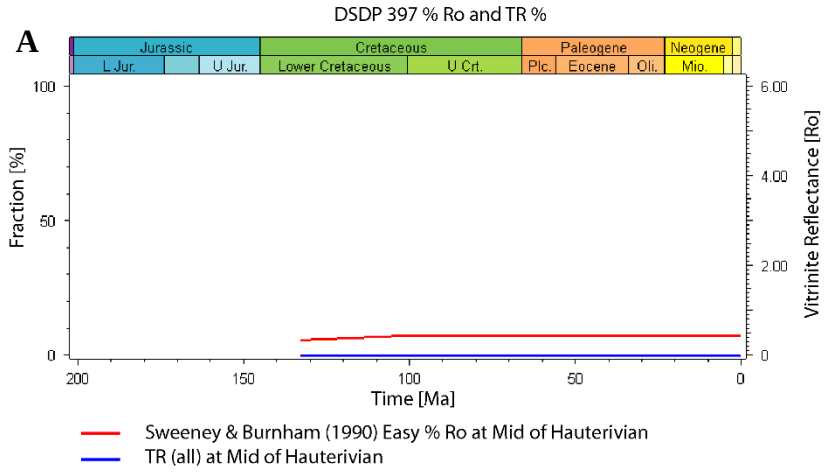
A
DSDP 397 % Ro and TR %
Jurassic
Cretaceous
Paleogene
Neogene
L Jur.
U Jur.
Lower Cretaceous
U Crt.
Plc.
Eocene
Oli.
Mio.
Fraction [%]
Vitrinite Reflectance [Ro]
Time [Ma]
Sweeney & Burnham (1990) Easy % Ro at Mid of Hauterivian
TR (all) at Mid of Hauterivian

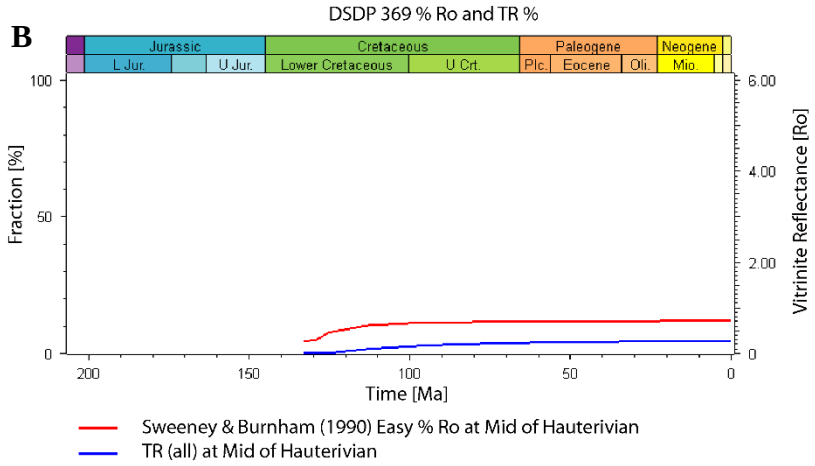
B
DSDP 369 % Ro and TR %
Jurassic
Cretaceous
Paleogene
Neogene
L Jur.
U Jur.
Lower Cretaceous
U Crt.
Plc.
Eocene
Oli.
Mio.
Fraction [%]
Vitrinite Reflectance [Ro]
Time [Ma]
Sweeney & Burnham (1990) Easy % Ro at Mid of Hauterivian
TR (all) at Mid of Hauterivian

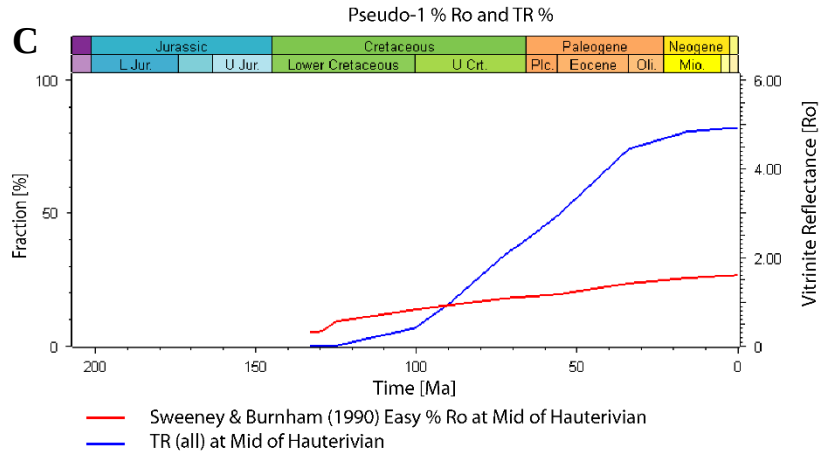
C
Pseudo-1 % Ro and TR %
Jurassic
Cretaceous
Paleogene
Neogene
L Jur.
U Jur.
Lower Cretaceous
U Crt.
Plc.
Eocene
Oli.
Mio.
Fraction [%]
Vitrinite Reflectance [Ro]
Time [Ma]
Sweeney & Burnham (1990) Easy % Ro at Mid of Hauterivian
TR (all) at Mid of Hauterivian

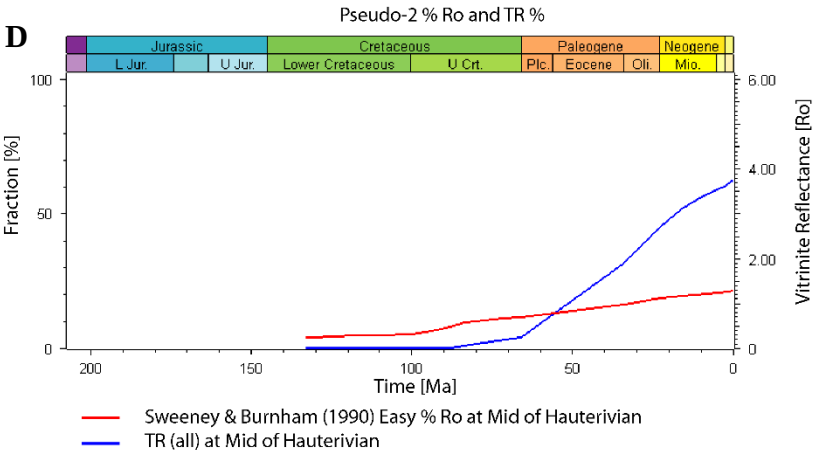
D
Pseudo-2 % Ro and TR %
Jurassic
Cretaceous
Paleogene
Neogene
L Jur.
U Jur.
Lower Cretaceous
U Crt.
Plc.
Eocene
Oli.
Mio.
Fraction [%]
Vitrinite Reflectance [Ro]
Time [Ma]
Sweeney & Burnham (1990) Easy % Ro at Mid of Hauterivian
TR (all) at Mid of Hauterivian

5. Discussion

Discussion of important observations made in this thesis are summarized below:

The absence of extensive evaporites in the TDB basin: While there is massive salt in the southern George's Bank Basin and the Baltimore Canyon area on the eastern North American conjugate margin of the Moroccan margin, previous workers and myself in this study of the TDB have not observed any significant evaporites along the southern margin of Morocco (Auxini, 1969; Von Rad and Einsele, 1980; Von Rad and Wissmann, 1982; Nemcok et al., 2005). Davison and Dailly (2010) mapped two discrete salt diapirs at the Aaiun area in the TDB that had not been detected by earlier mapping using an older vintage of 2D seismic data

The absence or minor salt occurrence in southern Morocco can be attributed to the high clastic sediment supply and subsidence rate at the southern Moroccan basins compared to the northern basins, which acted to prevent the precipitation of evaporites (Heyman, 1989). Heyman (1989) also proposed that the presence of a massive Jurassic carbonate platform inhibited the growth of salt structures and/or obscured their detection using seismic reflection methods.

Possible uplift at the base of the roll-over anticline in the passive margin fold belt: Interpretation of the seismic profile shown in Figure 6 revealed a localized uplift at the base of the roll-over anticline developed in the zone between the Jurassic and the top basement. Possible structural origins for this localized uplift include 1) Reactivation of preexisting, rift-related strike-slip faults in southern Morocco as the result of compressional inversion of the Atlas Mountains (Nemcok et al., 2005); or 2) the presence of a deeper, basal detachment surface at the basement

top along which the overlying sediments are sliding, folding the layers above, and forming a small bulge in the Jurassic section that can be observed on Figure 6. This second interpretation was also proposed by Hafid et al. (2008)

Obstruction of sediments transferred along the detachment: Sediment movement above the detachment by gravity sliding appears to be obstructed by an older, basement bulge that can be seen on the magnetic anomaly map in Figure 2. The basement bulge may obstruct the basinward flow of sediments and act as a nucleation point for the passive margin fold belt as proposed for the Lamu basin in offshore East Africa (Cruciani and Barchi, 2016; Cai et al., 2020)

Graded margin versus out-of-grade margins: Ross et al. (1994) proposed two types of continental margins based on their slope-to-basin profiles. The graded margins formed when the sediments prograde to the basin and aggrade upwards, while the out-of-grade margins form where the basin is over steepened, and sediment flow bypasses the slope and leads to margin erosion. Because of its long erosional history that began in the late Cretaceous, I consider the margin in the TDB as an out-of-grade margin.

Source rock maturity in the TDB. Source rock maturation and generation varies laterally through the TDB basin because of stratigraphic thickness changes and localized temperature and heat flow variations related to the type of underlying crust or depth-dependent variations in seawater temperatures (Figure 19). Using the modeled vitrinite reflectance values, I determined the present-day oil, wet gas, and dry gas windows estimated for the following modeling sites: DSDP well 397, DSDP well 369, and Pseudo-1 well.

Figure 19: Regional 2D seismic profile across the study area summarizing the extent and depth ranges of the present-day oil, wet gas, and dry gas windows based on estimates using modeled vitrinite reflectance values from DSDP well 397, DSDP 369, Pseudo-1 well and Pseudo-2 well. The **oil window** is interpreted as 0.6-1.1 Ro, the **wet gas window** as 1.1-1.3 Ro, and the **dry gas window** as 1.3-2.0 Ro. These maturity windows are found at greater depths below the seafloor in the deeper water areas of the study area because of crustal heat flow is lower in areas of oceanic crust, and colder bottom waters are present at those greater water depths.

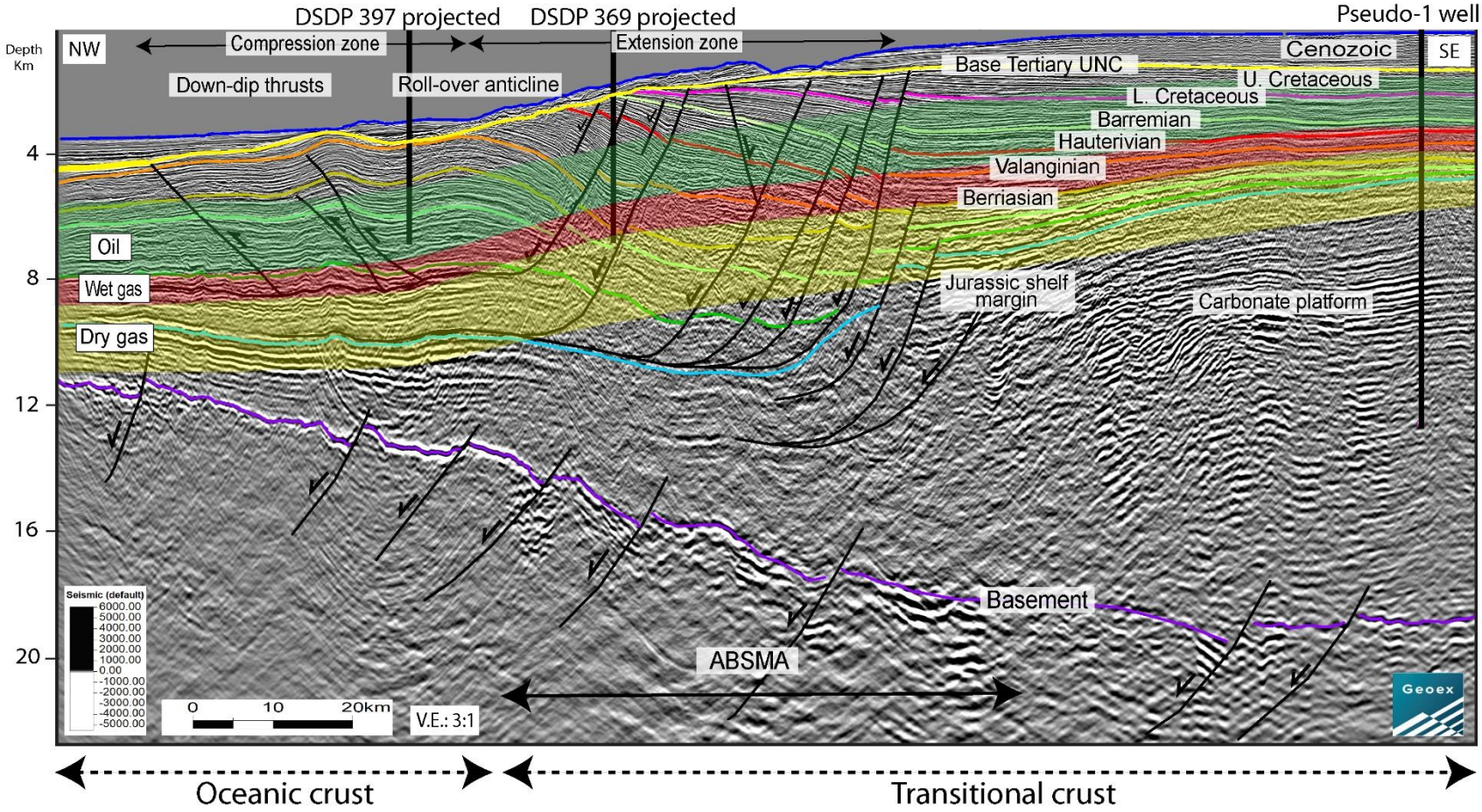
DSDP 397 projected
DSDP 369 projected
Pseudo-1 well
Depth Km
NW
SE
Compression zone
Extension zone
Down-dip thrusts
Roll-over anticline
Base Tertiary UNC
Cenozoic
U. Cretaceous
L. Cretaceous
Barremian
Hauterivian
Valanginian
Berriasian
Oil
Wet gas
Dry gas
Jurassic shelf margin
Carbonate platform
Basement
ABSMA
4
8
12
16
20
Seismic (default)
6000.00
5000.00
4000.00
3000.00
2000.00
1000.00
0.00
-1000.00
-2000.00
-3000.00
-4000.00
-5000.00
0
10
20km
V.E.: 3:1
Geoex
Oceanic crust
Transitional crust

The oil window for the TDB is interpreted as: 0.6-1.1 Ro; wet gas 1.1-1.3 Ro; and dry gas 1.3-2.0 Ro (Sweeney and Burnham, 1990). The maturity windows are deeper below the slope and basin due to cold bottom water flow and lower heat flow of oceanic basement while it is higher at the shelf due to the higher heat flow values and greater sediment thickness.

Petroleum system elements at the south: Basin modeling at the Pseudo-2 well modeling site indicated that the Lower Cretaceous, Hauterivian and Albian source rocks are at the late generative stage, and all these units started generation during the Paleocene. The presence of turbidites in the Lower Cretaceous basin floor fan and the Upper Cretaceous slope fan deposits could represent important stratigraphic reservoirs where hydrocarbons may migrate and be trapped in the landward-dipping strata along the slope (Figure 7).

6. Conclusions

1) The West Atlantic Coast Magnetic Anomaly (WACMA) of Morocco has been proposed as the early rift, African conjugate of the ECMA offshore North America. It forms a high magnetic anomaly parallel to the Moroccan shoreline that could be due to magmatic intrusions as dykes and sills during the breakup. While the African Blake Spur Magnetic Anomaly (ABSMA) is the African conjugate of the BSMA, it is mainly tilted half grabens filled with a post-rift magmatic flow that has high amplitude reflections.

2) The passive margin fold belt of the TDB, offshore southern Morocco, is 480-km-long and 68-km-wide. It is a gravity-driven, thin-skinned passive system formed by the gravitational gliding of sediments along regional detachment surface formed within the Jurassic sedimentary section. High clastic sediment supply within the Lower Cretaceous was fed by the Boujdour delta that led to loading and over steepening of the Cretaceous shelf-slope margin that, in turn, resulted in Cretaceous shelf failure and collapse to form the passive margin fold belt.

3) The passive margin offshore TDB is divided into two main zones: an up-dip extensional zone of listric normal faults, and a down-dip, rollover anticline with folds and thrusts at the distal compressional zone in the deepwater basin. The large folds within the fold belt are untested traps for hydrocarbons derived from the underlying mature Jurassic source rocks.

4) The estimated depth to detachment using area-depth-strain (ADS) analysis at the regional extension and compression zone is ± 9900 m, which matches the detachment depth that I interpreted from seismic profiles. The estimated depth to the detachment of the down-dip thrusts zone is 400 m deeper than the interpreted; this could be due to area loss at the shaly, ductile layers.

Another possible interpretation of the best-fit line at the down-dip thrusts zone indicates that there might be three consecutive detachments with three separate best-fit lines.

5) Basin modeling in the TDB showed that the Jurassic rocks are the main source rock responsible for the hydrocarbon generation in the TDB, and the hydrocarbon shows at the CB-1, Alisio 15 A-1, and Spansah 51 A-1 wells. Limited maturation and generation of the Lower Cretaceous source rocks in observed in some areas in the basin (Pseudo-1 and Pseudo-2 modeling sites).

6) Maturation and generation of the Lower Jurassic source rocks started as early as Upper Jurassic-Lower Cretaceous age. My basin modeling predicts that these Lower Jurassic source rocks are now over-mature, while the Hauterivian and Albian source rocks are immature. Although these younger sources could show some areas of localized maturation in certain parts of the TDB. The Upper Cretaceous source rocks are generally immature throughout the TDB.

BIBLIOGRAPHY

Arthur, M. A., U. von Rad, C. Cornford, F. McCoy, and M. Sarnthein, 1979, Evolution and Sedimentary History of the Cape Bojador Continental Margin, Northwestern Africa, *in* Initial Reports of the Deep Sea Drilling Project, 47 Pt. 1: U.S. Government Printing Office, p. 773–816.

Austin, J. A., P. L. Stoffa, J. D. Phillips, J. Oh, D. S. Sawyer, G. M. Purdy, E. Reiter, and J. Makris, 1990, Crustal structure of the Southeast Georgia embayment-Carolina trough: Preliminary results of a composite seismic image of a continental suture(?) and a volcanic passive margin: Geology, v. 18, no. 10, p. 1023–1027.

Auxini, A. E., 1969, Correlation estratigrafica de los sondeos perforados en el Sahara espanol: Bol.: Geol. Minero, Madrid., v. 83, p. 235–251.

Cai, J., Y. He, J. Liang, C. Qiu, and C. Zhang, 2020, Differential deformation of gravity-driven deep-water fold-and-thrust belts along the passive continental margin of East Africa and their impact on petroleum migration and accumulation: Marine and Petroleum Geology, v. 112, p. 104053.

Chamberlin, R. T., 1910, The Appalachian Folds of Central Pennsylvania: The Journal of Geology, v. 18, no. 3, p. 228–251.

Cool, T., B. Katz, T. Dignes, D. Reimers, and R. Fleisher, 2008, Hydrocarbon source rock assessment and revised biostratigraphy of DSDP Site 369A, offshore Northwest African margin: Journal of Petroleum Geology, v. 31, no. 2, p. 117–133.

Cruciani, F., and M. R. Barchi, 2016, The Lamu Basin deepwater fold-and-thrust belt: An example of a margin-scale, gravity-driven thrust belt along the continental passive margin of East Africa: Tectonics, v. 35, no. 3, p. 491–510.

Davison, I., 2005, Central Atlantic margin basins of North West Africa: Geology and hydrocarbon potential (Morocco to Guinea): Journal of African Earth Sciences, v. 43, no. 1–3, p. 254–274.

Davison, I., and P. Dailly, 2010, Salt tectonics in the Cap Boujdour Area, Aaiun Basin, NW Africa: Marine and Petroleum Geology, v. 27, no. 2, p. 435–441.

Eichelberger, N. W., A. G. Nunns, C. Reilly, R. Dirkx, Y. Yarbuh, and D. Bate, 2017, Quantitative Structural Analysis of Newly Acquired Data From Mexican Ridges Fold Belt, Western Gulf of Mexico. presentation.: www.structuresolver.com/case-studies/mexican-ridges-presentation.

Epard, J. L., and R. H. Groshong Jr., 1993, Excess Area and Depth to Detachment: AAPG Bulletin, v. 77, no. 8, p. 1291–1302.

Esri, GEBCO, NOAA, Garmin, HERE, and other contributors., 2014, World Ocean Base: www.arcgis.com/home/item.html?id=1e126e7520f9466c9ca28b8f28b5e500.

Fiduk, J. C. et al., 1999, The Perdido Fold Belt, Northwestern Deep Gulf of Mexico, Part 2: Seismic Stratigraphy and Petroleum Systems: AAPG Bulletin, v. 83 (1999), no. 4, p. 578–612.

GEBCO, 2009, GEBCO_08 Grid: A global 30 arc-second grid, British Oceanographic Data Centre.: www.gebco.net/news_and_media/updated_gebco_08_release.

Gesamtfakult, N., A. Adrian, O. Wenke, H. Altstadt, and A. A. O. Wenke, 2014, Sequence stratigraphy and basin analysis of the Meso- to Cenozoic Tarfaya- Laâyoune Basins , on- and offshore Morocco, Phd thesis: Ruprecht-Karls-Universität Heidelberg,

Gradstein, F. M., J. G. Ogg, A. G. Smith, W. Bleeker, and L. J. Lourens, 2004, A new Geologic Time Scale, with special reference to Precambrian and Neogene: Episodes, v. 27, no. 2, p. 83–100.

Groshong, R. H., and J. L. Epard, 1994, The role of strain in area-constant detachment folding: Journal of Structural Geology, v. 16, no. 5, p. 613–618.

Hafid, M., G. Tari, D. Bouhadioui, I. El Moussaid, H. Echarfaoui, A. A. Salem, M. Nahim, and M. Dakki, 2008, Atlantic Basins, *in* G. S. Bhattacharji, Brooklyn H. J. Neugebauer, Bonn J. Reitner, Göttingen K. Stüwe, ed., Continental Evolution: The Geology of Morocco. Lecture Notes in Earth Sciences: Springer Berlin Heidelberg, p. 303–329.

Hasterok, D., 2013, A heat flow based cooling model for tectonic plates: Earth and Planetary Science Letters, v. 361, p. 34–43.

Hayes, D. E., A. C. Pimm, J. P. Beckmann, W. E. Benson, W. H. Berger, P. H. Roth, P. R. Supko, and U. von Rad, 1972, Site 139, *in* Initial Reports of the Deep Sea Drilling Project, 14: U.S. Government Printing Office, p. 2973.

Heyman, M. A. W., 1989, Tectonic and depositional history of the Moroccan continental margin: : Chapter 21: European-African Margins, *in* A. J. Tankard, and H. R. Balkwill, eds., Extensional tectonics and stratigraphy of the North Atlantic margins: AAPG Memoir, p. 323–340.

Holik, J. S., P. D. Rabinowitz, and J. A. Austin, 1991, Effects of Canary hotspot volcanism on structure of oceanic crust off Morocco: Journal of Geophysical Research, v. 96, no. B7, p. 12039–12067.

Hyndman, R. D., M. G. Langseth, and R. P. Von Herzen, 1987, Deep Sea Drilling Project geothermal measurements: A review: Reviews of Geophysics, v. 25, no. 8, p. 1563–1582.

Keller, F., J. L. Meuschke, and L. R. Alldredge, 1954, Aeromagnetic surveys in the Aleutian, Marshall, and Bermuda Islands: Eos, Transactions American Geophysical Union, v. 35, no. 4, p. 558–572.

Kendrick, J. W., A. Hood, and J. R. Castano, 1978, Petroleum-Generating Potential of Sediments from Leg 41, Deep Sea Drilling Project, *in* Initial Reports of the Deep Sea Drilling Project, 41: U.S. Government Printing Office, p. 1–21.

Klingelhoefer, F., C. Labails, E. Cosquer, S. Rouzo, L. Geli, D. Aslanian, J.-L. Olivet, M. Sahabi, H. Nouze, and P. Unternehr, 2009, Crustal structure of the SW-Moroccan margin from wide-angle and reflection seismic data (The DAKHLA experiment) Part A : Wide-angle seismic models .: Tectonophysics, v. 468, p. 63–82.

Klitgord, K. D., and H. Schouten, 1986, Plate kinematics of the central Atlantic, *in* P. R. Vogt, and B. E. Tucholke, eds., The Western North Atlantic Region: North America, Geology of North America, Geological Society of America, p. 351–378.

Krueger, A., and E. Gilbert, 2009, Deepwater Fold-Thrust Belts : Not All the Beasts Are Equal: AAPG Search and Discovery, v. 30085, p. 1–6.

Labails, C., J.-L. Olivet, D. Aslanian, and W. R. Roest, 2010, An alternative early opening scenario for the Central Atlantic Ocean: Earth and Planetary Science Letters, v. 297, no. 3–4, p. 355–368.

Labails, C., J.-L. Olivet, and The Dakhla study group, 2009, Crustal structure of the SW Moroccan margin from wide-angle and reflection seismic data (the Dakhla experiment). Part B - The tectonic heritage: Tectonophysics, v. 468, no. 1–4, p. 83–97.

Lawrence, S., 2019, Atlantic Offshore Morocco New Data, New Insights: GeoExpro Magazine, v. 16, no. 3, p. 60–62.

Maloney, D., R. Davies, J. Imber, and S. King, 2012, Structure of the footwall of a listric fault system revealed by 3D seismic data from the Niger Delta: Basin Research, v. 24, no. 1, p. 107–123.

Morley, C. K., R. King, R. Hillis, M. Tingay, and G. Backe, 2011, Deepwater fold and thrust belt classification, tectonics, structure and hydrocarbon prospectivity: A review: p. 41–91.

Nemcok, M., C. Stuart, M. P. Segall, R. B. Allen, C. Christensen, S. A. Hermeston, and I. Davison, 2005, Structural Development of Southern Morocco: Interaction of Tectonics and Deposition, *in* P. Post, N. Rosen, D. Olson, S. L. Palmes, K. T. Lyons, and G. B. Newton, eds., Petroleum Systems of Divergent Continental Margin Basins: 25th Annual, Houston, Texas, SEPM Society for Sedimentary Geology, p. 151–202.

Neumaier, M., S. Back, R. Littke, P. A. Kukla, M. Schnabel, and C. Reichert, 2016, Late Cretaceous to Cenozoic geodynamic evolution of the Atlantic margin offshore Essaouira (Morocco): Basin Research, v. 28, no. 5, p. 712–730.

Olsen, P. E., D. V. Kent, M. Et-Touhami, and J. Puffer, 2003, Cyclo-, magneto-, and bio-stratigraphic constraints on the duration of the CAMP event and its relationship to the Triassic-Jurassic boundary, *in* Geophysical Monograph Series: Blackwell Publishing Ltd, p. 7–32.

ONHYM, 2019, Opportunities for hydrocarbons exploration and production in Morocco, Boujdour: handout: San Antonio, USA, AAPG International Conference and Exhibition, 19-22 May, 1–19 p.

Patriat, M., and C. Labails, 2006, Linking the Canary and Cape-Verde hot-spots, Northwest Africa: Marine Geophysical Research, v. 27, no. 3, p. 201–215.

Pyles, D. R., J. P. M. Syvitski, and R. M. Slatt, 2011, Defining the concept of stratigraphic grade and applying it to stratal (reservoir) architecture and evolution of the slope-to-basin profile: An outcrop perspective: Marine and Petroleum Geology, v. 28, no. 3, p. 675–697.

Von Rad, U., and G. Einsele, 1980, Mesozoic--Cainozoic Subsidence History and Palaeobathymetry of the Northwest African Continental Margin (Aaiun Basin to D. S. D. P. Site 397): Philosophical Transactions of the Royal Society of London. Series A, Mathematical and Physical Sciences, v. 294, no. 1409, p. 37–50.

Von Rad, Ulrich, and G. Wissmann, 1982, Cretaceous-Cenozoic History of the West Saharan Continental Margin (NW Africa): Development, Destruction and Gravitational Sedimentation, *in* U. Von Rad, K. Hinz, M. Sarnthein, and E. Seibold, eds., Geology of the Northwest African Continental Margin: Springer Berlin Heidelberg, p. 106–131.

Von Rad, U., and M. Sarti, 1986, Early Cretaceous »events« in the evolution of the eastern and western North Atlantic continental margins: Geologische Rundschau, v. 75, no. 1, p. 139–158.

Roeser, H. A., 1982, Magnetic anomalies in the magnetic quiet zone off Morocco., *in* U. von Rad, K. Hinz, M. Sarnthein, and E. Seibold, eds., Geology of the northwest African continental margin: Springer, Berlin Heidelberg, p. 61–68.

Rowan, M. G., F. J. Peel, and B. C. Vendeville, 2004, Gravity-driven Fold Belts on Passive Margins, *in* K. R. McClay, ed.,Thrust Tectonics and Hydrocarbon Systems: American Association of Petroleum Geologists, p. 159–184.

Le Roy, C., C. Rangin, X. Le Pichon, H. N. Thi Ngoc, L. Andreani, and M. Aranda-Garcia, 2008, Neogene crustal shear zone along the western Gulf of Mexico margin and its implications for gravity sliding processes. Evidences from 2D and 3D multichannel seismic data: Bulletin de la Société Géologique de France, v. 179, no. 2, p. 175–193.

Sachse, V. F., A. Wenke, R. Littke, H. Jabour, O. Kluth, and R. Zühlke, 2016, 2D petroleum system analysis of the Tarfaya Basin, on-offshore Morocco, North Africa: Marine and Petroleum Geology, v. 77, p. 1108–1124.

Shipboard Scientific Party, 1979, Site 397, *in* U. Von Rad, and W. B. F. Ryan, eds., Initial Reports of the Deep Sea Drilling Project, 47 Pt. 1: U.S. Government Printing Office, p. 17–217.

Srivastava, S. P., and C. R. Tapscott, 1986, Plate kinematics of the North Atlantic, in P.R. Vogt and B.E. Tucholke,eds.: The western North Atlantic region: The geology of North America Geological society of America, p. 379–404.

Sweeney, J. J., and A. K. Burnham, 1990, Evaluation of a simple model of vitrinite reflectance based on chemical kinetics: American Association of Petroleum Geologists Bulletin, v. 74, no. 10, p. 1559–1570.

Talwani, Manik, J. Ewing, R. E. Sheridan, W. S. Holbrook, and L. Glover, 1995, The Edge Experiment and the U.S. East Coast Magnetic Anomaly, *in* E. Banda, M. Torné, and M. Talwani, eds., Rifted Ocean-Continent Boundaries. NATO ASI Series (Series C: Mathematical and Physical Sciences), vol 463.: Springer Netherlands, p. 155–181.

The Shipboard Scientific Party, 1978, Site 369: Continental Slope off Cape Bojador, Spanish Sahara, *in* Initial Reports of the Deep Sea Drilling Project, 41: U.S. Government Printing Office, p. 327–420.

Weigel, W., G. Wissmann, and P. Goldflam, 1982, Deep Seismic Structure (Mauritania and Central Morocco), *in* U. von Rad, K. Hinz, M. Sarnthein, and E. Seibold, eds., Geology of the Northwest African Continental Margin: Springer Berlin Heidelberg, p. 132–159.

Wygrala, B., 1989, Integrated Study of an Oil field in the Southern Po Basin, Northern Italy: (No. FZJ-2014-03033). Publikationen vor 2000, p. 328.